AN ABSTRACT OF THE THESIS OF

Harish V. Peddibhotla for the degree of Master of Science in

Electrical and Computer Engineering presented on December 12, 2005.

Title: New Configurations for RF/Microwave Bandstop and Lowpass Filters.

Abstract approved:

_____

Raghu Kumar Settaluri

This thesis presents new, compact configurations for RF/microwave
bandstop and lowpass filters for embedded passive applications. A simple
design methodology is presented for designing the folded-transmission line
filters on a microstrip platform. Unlike the conventional stub-loaded filter
designs, the proposed folded-line filters will have practical dimensions for a
wide range of electrical specifications, making physical implementation
realizable.

Further compactness is achieved by folding the transmission lines in a
multi-layered environment. A back-to-back microstrip with through-holes in the
ground plane is considered for this purpose. Closed-form design equations for
the frequency independent R, L, C components have been developed for
implementation in the circuit model of the through-ground via. The proposed

configurations offer significant footprint reduction compared to the conventional geometries. Several lowpass and bandstop filters are designed in single and multi-layered environments, and the theoretical response is validated by full-wave EM simulation as well as with measurement.

New Configurations for RF/Microwave Bandstop and Lowpass Filters

by

Harish V. Peddibhotla

A THESIS

submitted to

Oregon State University

in partial fulfillment of
the requirements for the
degree of

Master of Science

Presented December 12, 2005
Commencement June 2006

Master of Science thesis of <u>Harish V. Peddibhotla</u> presented on
<u>December 12, 2005.</u>

APPROVED:

_____

Major Professor, representing Electrical Engineering and Computer Science

_____

Director of the School of Electrical Engineering and Computer Science

_____

Dean of the Graduate School

I understand that my thesis will become part of the permanent collection of

Oregon State University libraries. My signature below authorizes release of my

thesis to any reader upon request.

_____

Harish V. Peddibhotla, Author

ACKNOWLEDGEMENTS

Kolstad and Yevgeny Mayevisky for their useful discussions and participation in group projects.

I would also like to thank Ferne Simendinger, April Melton and the staff of the Electrical Engineering and Computer Science, Graduate School and the Office of International Education departments for their assistance during my stay at Oregon State University.

I would particularly like to thank my parents in India for their constant encouragement and support. Finally I would like to thank my friends in Corvallis for making my stay memorable.

TABLE OF CONTENTS

TABLE OF CONTENTS (Continued)

LIST OF FIGURES

LIST OF FIGURES (Continued)

LIST OF FIGURES (Continued)

LIST OF FIGURES (Continued)

LIST OF TABLES

NEW CONFIGURATIONS FOR RF/MICROWAVE BANDSTOP AND LOWPASS FILTERS

1. INTRODUCTION

1.1 Background

High-speed mixed integrated circuits are playing a major role in wireless and mobile communication devices today. The increasing clock rates, higher packaging densities, compact geometries and the overall complexity have been some of the major concerns for the RF, microwave design engineer. The demand for shorter development cycles and expedited time-to-market requires the engineer to come up with quick design solutions.

Implementation of embedded integrated passive components in multilayer low temperature co-fired ceramics (LTCC) is one of the recent trends in the technology [1], [2]. Some of the significant advantages of LTCC are low dielectric losses at RF/microwave frequencies and better-controlled dielectric properties. Multi-chip module deposition is another popular System-on-Package (SOP) technology [3], [4] that employs high-performance embedded passives. The deployment of embedded passives in multi-layered media has provided an attractive alternative to the implementation of off-chip passive components in RF and mixed signal circuits. Among passive components, bandstop and lowpass filters are used for a variety of wireless applications. In particular, lowpass filters with low insertion loss and high stop band attenuation are used to suppress spurious signals and harmonics. Bandstop

filters are employed to reject selected frequency bands. These filters find frequent applications in mixers, oscillators, equalizers and other communication systems.

A basic block diagram for an RF wireless transceiver for personal communications is shown in Fig. 1.1. In the receiver mode, the signal received by the antenna is filtered to select the RF band of interest, after which it is fed into the Low Noise Amplifier (LNA). The signal is then usually filtered with the help of a lowpass filter (LPF) or a bandstop filter (BSF) to remove the unwanted frequency bands, followed by mixing directly to the baseband or mixing to one or more intermediate frequencies (IF) . Often the last mixing operation will separate the signal into its independent I and quadrature Q components. Once at baseband, the signal will be converted to digital and then processed.
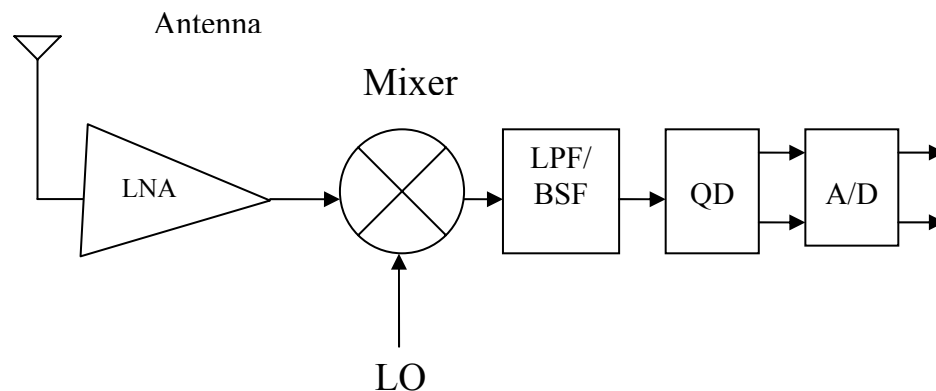
Fig. 1.1 RF Wireless Transceiver Block Diagram

1.2   Limitations of the Conventional Filter Designs

Some of the conventional filter configurations employing transmission line sections are the stepped impedance filters, coupled line filters, filters using coupled resonators and stub-loaded filters [5] - [8]. Stub-loaded lowpass filters can be designed with the length of the transmission line sections being $\lambda/8$, where λ is the wavelength at the specified frequency. Similarly, stub-loaded bandstop filters can be designed with the length of the transmission line sections being $\lambda/4$.

However, in the lower microwave frequency range (1-10 GHz), the conventional transmission line filter theory [5] - [8] results in large component footprints, as the wavelength λ is large at these frequencies. Further, some of the conventional filter designs (for example stub-loaded bandstop and lowpass filters) can often lead to very large/small values of the characteristic impedances, making the physical implementation unrealizable.

1.3   Motivation for Research

The transmission line sections of the conventional filter geometries can be folded in a multi-layer, multi-conductor environment to achieve greater reduction in the footprint [9] - [12]. Further, the folded line designs have convenient physical dimensions for a practical realization, thus eliminating the problem of having very narrow or very wide line widths, as in the case of the conventional filter configurations. Fig. 1.2 depicts some of the possible folded-

line configurations for the filter sections. The effect of mutual coupling between the lines, curved line sections and the interconnecting lengths of the sections can be taken into account to obtain the network parameters of the folded-line filter sections. These filter sections can be cascaded to give the overall filter response.

The other motivating factors for the research include the use of one common design methodology for designing bandstop and lowpass filters and the use of the existing conventional filter theory in the first phase of the design of the folded line filters.

Conventional
lowpass/bandstop

Single-level folded line
lowpass/bandstop

(a)

Top metal layer

Bottom metal layer

Conventional
lowpass/bandstop

Single-level folded line
lowpass/bandstop

Multi-level folded line
lowpass/bandstop

(b)
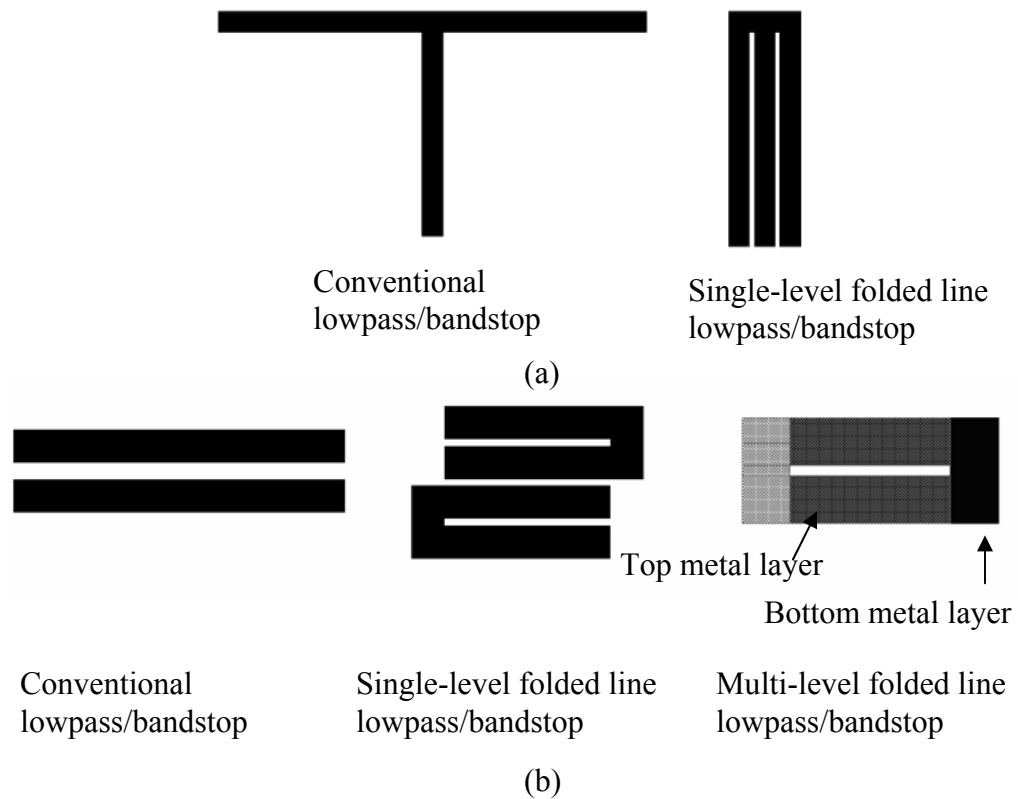
Fig. 1.2 Possible configurations for the folded-line filter sections (a) Stub-loaded (b) Gap-coupled

1.4 Organization of the Study

This research focuses on the realization of new, compact configurations for bandstop and lowpass filters in single and multi-layer environments. Unlike the conventional filter configurations, these new filter configurations have convenient physical dimensions for a practical realization.

Chapter 2 provides a brief description of the conventional filter theory for lowpass and bandstop filters. The two main methods used in filter design, namely image parameter method and the insertion loss method, are highlighted and the latter explained in detail. The criteria involved in the selection of the filter response type (maximally flat/Chebyshev) are addressed. The relevance of parameters such as the cut-off /center frequency and 3-dB bandwidth, used in any filter design, is highlighted.

Chapter 3 presents several new, compact topologies for multiple coupled folded line bandstop and lowpass filters in a single layer configuration. A simple design procedure is described for designing these filters on a microstrip platform. The reduced two-port network parameters for the filter sections are obtained from a network representation of the folded line structures. The effects of the mutual coupling between the transmission lines, curved line sections and the interconnecting lengths of the sections are taken into account for obtaining the network parameters.

Chapter 4 presents new, compact topologies for multiple coupled folded line bandstop and lowpass filters in a multi-layer configuration. This

chapter emphasizes the fact that the overall footprint of the filters can be greatly reduced by folding the transmission line sections onto different layers. This also facilitates an increased density and reduces the effect of edge coupling between the straight and curved transmission line sections as they are now folded onto different layers. These multi-layer filters have been implemented in a back-to-back microstrip configuration. The ground plane sandwiched between the dielectric layers serves to sufficiently isolate the transmission lines on either side of the ground plane. Through-ground via models have been developed to interconnect the top and bottom metallization layers.

Chapter 5 presents experimental validation for the bandstop and lowpass folded line filters. The bandstop and lowpass filters on a single layer were implemented on a conventional microstrip platform, while those on a multi-layer configuration were implemented on a back-to-back microstrip platform. This chapter presents the measurement results in comparison with the theoretical results, as well as with full wave EM simulation.

Chapter 6 presents the conclusions drawn from this study and potential avenues for further research in this field of filter synthesis and design.

2. CONVENTIONAL FILTER THEORY

2.1   Introduction

A filter is a two-port network, which controls the frequency response by allowing transmission in the passband and attenuation in the stopband. Filters are used for a variety of applications, including separation and addition of signals of different frequencies, impedance matching networks, coupling networks for microwave tubes, negative resistance amplifiers, time–delay networks, slow-wave structures and in the general design of microwave components. Microwave filters are usually modeled either as waveguide filters, including cavity filters [6], [13], [14], or as microstrip or stripline filters [5] - [8]. Some of the common transmission line filters are the stub loaded filters, stepped impedance filters, coupled line filters, and coupled resonator filters respectively [5] ,[6], [7], [13], [14].

2.2   Filter Classification

The most common classification of filters can be in terms of their type: lowpass, highpass, bandpass and bandstop. The ideal filter responses are shown in Fig. 2.1-2.4. The attenuation in dB is plotted as a function of frequency in Fig. 2.1-2.4. The attenuation is zero in the passband and infinite attenuation is observed in the stopband. The cut-off frequency is denoted by f_c and the band-edge frequencies are denoted by f_1 and f_2 respectively.

8
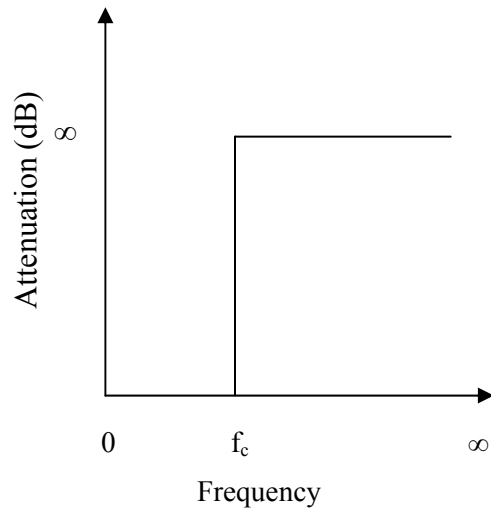
Fig 2.1 Ideal lowpass filter
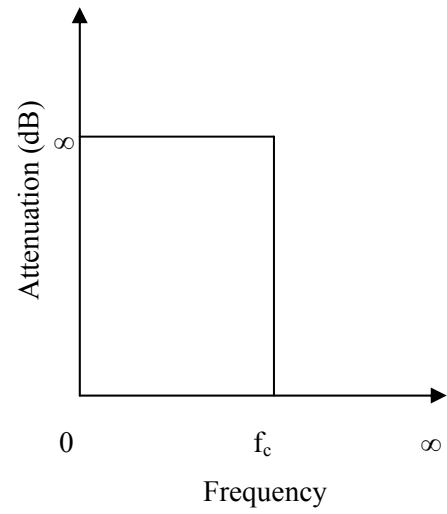
Fig 2.2 Ideal highpass filter
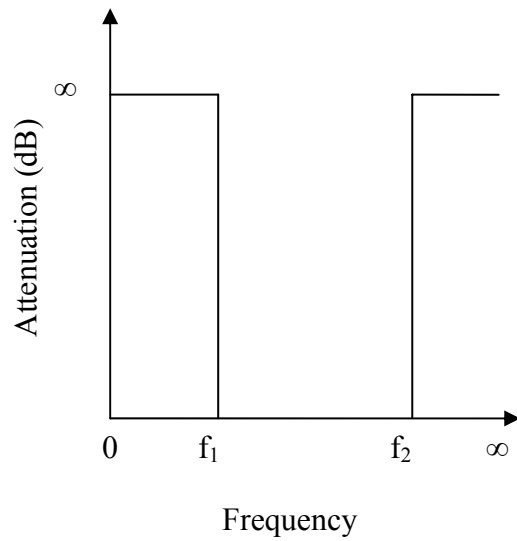
Fig 2.3 Ideal bandpass filter
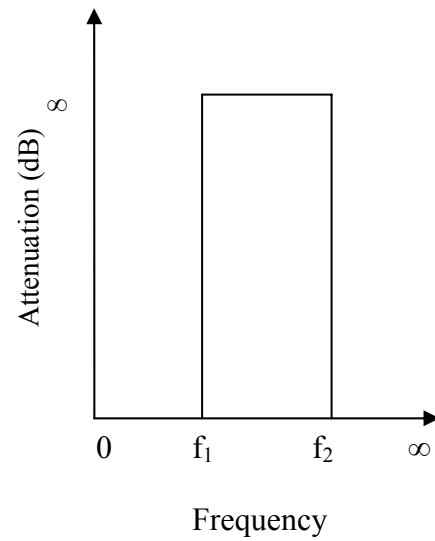
Fig 2.4 Ideal bandstop filter

In order to suppress spurious signals or harmonics, lowpass filters with low insertion loss and high attenuation are employed. A highpass filter is essentially a complement of the lowpass filter. Bandstop filters are used to reject selected frequency bands whereas bandpass filters allow selected bands of frequencies and reject frequencies both above and below the passband. These filters find frequent applications in mixers, oscillators, equalizers, multiplexers and other communication systems.

2.3 Filter Design Methodology

Two primary methods used in the design of microwave filters are the image parameter method and the insertion loss method [5] - [7]. Analogous to the plane wave concept used for the analysis of transmission lines, the image concept can also be viewed from a plane wave standpoint. For a uniform transmission line, the characteristic impedance is also the same as the image impedance. This design involves the specification of the passband and stopband characteristics for a cascade of two-port networks. The image parameter method is useful for simple filters and provides a link between the infinite periodic structures and practical filter structures. The image parameter method is not a part of this research and thus will not be considered.

The insertion loss method allows a high degree of control over the passband and stopband amplitude and phase characteristics, thereby providing a systematic way to synthesize the desired response. When a minimum insertion

loss is needed, a binomial response can be used (also known as maximally flat or Butterworth response). On the other hand, when a sharp cutoff response is needed with a possible allowable ripple, a Chebyshev response is the appropriate choice. A better phase response while sacrificing the attenuation rate can be obtained by using a linear phase filter design. All the above requirements can be met by using the insertion loss method with the use of a higher order filter.

In the insertion loss method, a filter response is defined by its insertion loss, or power loss ratio, P_{LR}, where the equation for the power loss ratio is given as

$$P_{LR} = \frac{Power\ available\ from\ the\ source(P_{inc})}{Power\ \text{delivered to the load}(P_{load})} = \frac{P_{inc}}{P_{load}} = \frac{1}{1-|\Gamma(\omega)|^2} \qquad (2.1)$$

Here $\Gamma(\omega)$ is defined as the reflection coefficient expressed as a function of the angular frequency, the reflection coefficient representing the mismatch between the source impedance and the input impedance of the filter network. The power loss ratio is the reciprocal of $|S_{21}|^2$ if both the load and the source are matched and the filter is lossless. The insertion loss (IL) in dB is given as

$$IL = 10\ \log\ (P_{LR}) \qquad (2.2)$$

Since $|\Gamma(\omega)|^2$ is an even function of ω, it can therefore be expressed as a polynomial in ω^2. It can be written as shown in equation 2.3.

$$|\Gamma(\omega)|^2 = \frac{M(\omega^2)}{M(\omega^2)+N(\omega^2)} \qquad (2.3)$$

where M and N are real polynomials in ω^2. Substituting equation (2.3) in equation (2.1) gives

$$P_{LR} = 1 + \frac{M(\omega^2)}{N(\omega^2)} \qquad (2.4)$$

The power loss ratio must be of a form similar to equation (2.4) for a filter to be physically realizable. This automatically places a constraint on the reflection coefficient $\Gamma(\omega)$. Some of the practical filter responses are the maximally flat, equal ripple and linear phase, respectively. The maximally flat response, also called the binomial or the Butterworth response is optimum in the sense that it provides the flattest possible passband response for a given filter order. For a lowpass filter, the equation is

$$P_{LR} = 1 + k^2 (\tfrac{\omega}{\omega_c})^{2N} \qquad (2.5)$$

where the order of the filter is represented by N and ω_c is the cutoff frequency. The passband extends from ω=0 to ω=ω_c. At the band edge ω=ω_c, the power loss ratio is $1+k^2$. The -3 dB point is chosen here, therefore k=1. The -3 dB point is also called the half power point. For ω>ω_c, the attenuation increases monotonically with frequency as shown in Fig. 2.5. For ω>>ω_c, the insertion loss increases at the rate of 20N dB/decade. The first (2N-1) derivatives are zero at ω=0, and this is similar to the binomial response for multisection quarter-wave transformers. For an Nth order low-pass filter, if a Chebyshev polynomial is used to specify the insertion loss, the resulting equation is

$$P_{LR} = 1 + k^2 T_N^{\,2}(\tfrac{\omega}{\omega_c}) \qquad (2.6)$$

A sharper cutoff will result although the passband response will have ripples of amplitude $1+k^2$ as shown in Fig. 2.5. This is because the Chebyshev polynomial $T_N(x)$ oscillates between ± 1 for $|x| \leq 1$. Thus, the passband ripple level is determined by k^2. For large x, $T_N(x) \cong \frac{1}{2(2x)^N}$ so for $\omega >> \omega_c$, the insertion loss becomes $P_{LR} \cong \frac{k^2}{4}(\frac{2\omega}{\omega_c})^{2N}$, which also increases at the rate of 20N dB/decade. At any given frequency where $\omega >> \omega_c$, the insertion loss for the Chebyshev response is $(2^{2N})/4$ greater than for the binomial response.

The insertion loss method of filter design starts with the low-pass filter prototypes, which are normalized in terms of impedance and frequency. The normalization simplifies the filter design for an arbitrary frequency, impedance, and filter type (low-pass, high-pass, bandpass and bandstop). The low-pass prototypes are then scaled to the desired frequency and impedance. For implementation at microwave frequencies, the lumped element components are replaced with the distributed elements. The process of filter design by the insertion loss method is shown in Fig. 2.6.

Depending on the type of the response specified (Maximally flat or Chebyshev or equal-ripple) the first step is to start with the low-pass filter prototype. For a normalized lowpass design where the source impedance is 1Ω and the cutoff frequency is $\omega_c=1$ rad/sec, the element values for the ladder type circuits are available [5], [6]. The normalized lowpass design is the starting point for designing lowpass, highpass, bandpass and bandstop filters respectively.

P_{LR}

Equal
Ripple

Maximally
Flat

$1+k^2$

1

0   0.5   1.0   1.5 ω/ω_c
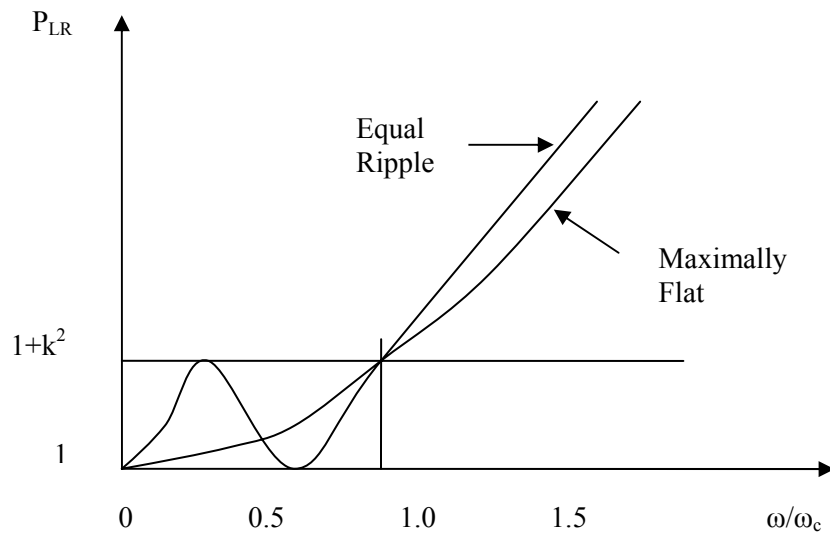
Fig. 2.5 Maximally flat and equal ripple low-pass filter responses (N=3)

| Filter specifications | Low-pass prototype design | Scaling and conversion | Implementation |
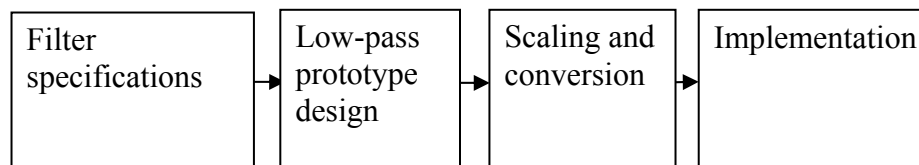
Fig. 2.6 Filter design procedure using the insertion loss method

As shown in Fig. 2.7, the element values are numbered from g_0 at the generator impedance to g_{N+1} at the load impedance, for a filter having N reactive elements. The elements alternate between series and shunt connections and g_k has the following definition:

g_0= {generator resistance (Fig. 2.7a)

generator conductance (Fig. 2.7b)}

g_k= {inductance for series inductors (k=1 to N)

capacitance for shunt capacitors (k=1 to N)}

g_{N+1}= {load resistance if g_N is a shunt capacitor

load conductance if g_N is a series inductor}.

The lowpass filter prototype element values, the g's are readily available in literature [5], [6]. Depending on the lowpass filter prototype (maximally flat/ Chebyshev, cut-off frequency, order of the filter etc.), the corresponding values of the g's can be obtained [5], [6].

The circuits of Fig 2.7 are considered dual of each other and both will give the same response. The size or the order of the filter needs to be determined to design the filter. The insertion loss at some frequency in the stopband of the filter is specified for this. For an equal-ripple low-pass filter with a cutoff frequency ω_c=1, the power loss ratio is given by the equation:

$$P_{LR} = 1 + k^2 T_N{}^2(\omega) \tag{2.7}$$

where P_{LR} refers to the power loss ratio, k is the multiplication factor and T_N refers to the Chebyshev polynomial [5] [6]. The power loss ratio was defined in equation 2.1 and the insertion loss S_{21} can be expressed in terms of the power loss ratio as expressed in equation 2.2. The insertion loss is an important quantity in any filter design.
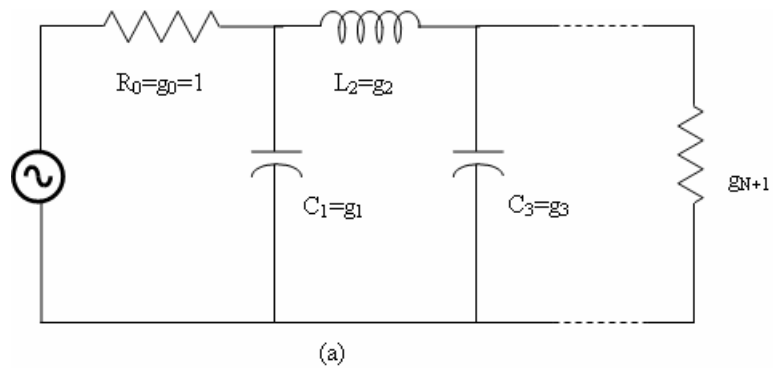
(a)
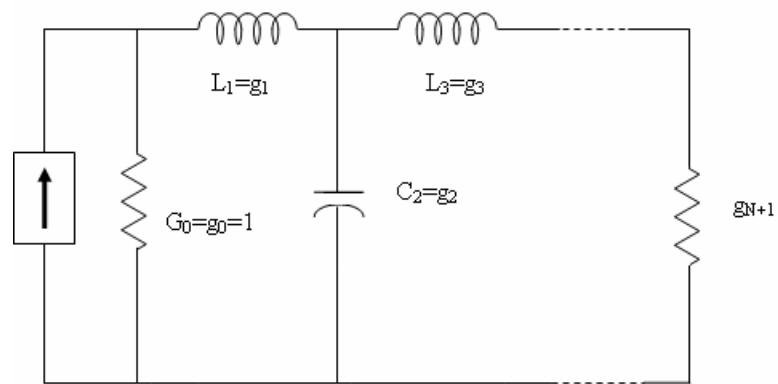
(b)

Fig. 2.7   Ladder circuits for low-pass filter prototypes
a) First element is a shunt capacitor
b) First element is a series inductor

$1+k^2$ in equation 2.7 denotes the ripple level in the passband. The Chebyshev polynomial has the following property:

$$T_N(0) = \{0 \text{ for N odd}$$

$$1 \text{ for N even}\}$$

The power loss ratio is unity at $\omega=0$ for N odd, but is equal to $1+k^2$ at $\omega=0$ for N even. Tables exist [6], [7] for designing equal-ripple low-pass filters

with a normalized source impedance and cutoff frequency ($\omega_c{}' = 1$) and can be applied to any of the ladder circuits of Fig. 2.7. A point to be noted is that $g_{N+1} \neq 1$ for even N. If the stopband attenuation is specified, the necessary value of N can be determined from the ripple values.

The low-pass prototypes, as explained earlier, are normalized designs having a source impedance of $R_s = 1\Omega$ and a cutoff frequency of $\omega_c = 1$. These designs can be scaled in terms of impedance and frequency and can then be converted to give high-pass, bandpass or bandstop characteristics. The prototype design has the source and load impedances of unity (the only exception being equal-ripple filters with even N, which have non-unity load resistance). By multiplying the impedance of the prototype design by R_0, a source resistance of R_0 can be obtained. The impedance-scaled quantities for the new filter component denoted by primes here are given by the following equations:

$$L' = R_0 L \tag{2.8}$$

$$C' = \frac{C}{R_0} \tag{2.9}$$

$$R_S' = R_0 \tag{2.10}$$

$$R_L' = R_0 R_L \tag{2.11}$$

where the L, C, and R_L are the component values of the original prototype. To change the cutoff frequency of a lowpass prototype from unity to ω_c, we have to scale the frequency dependence of the filter by the factor $1/\omega_c$. This is done by replacing ω by ω/ω_c. The new power loss ratio will be given by:

$$P_{LR}'(\omega) = P_{LR}(\tfrac{\omega}{\omega_c}) \tag{2.12}$$

Here ω_c is the new cutoff frequency, the cutoff occurring when $\omega/\omega_c=1$, or $\omega=\omega_c$. Replacing ω by ω/ω_c, the series reactances (X_k) and the shunt susceptances (B_k) are modified as:

$$jX_k = j\tfrac{\omega}{\omega_c} L_k = j\omega L_k' \quad \text{and} \quad jB_k = j\tfrac{\omega}{\omega_c} C_k = j\omega C_k' \tag{2.12a}$$

Therefore, the new element values are modified correspondingly

$$L_k' = \tfrac{L_k}{\omega_c} \tag{2.13}$$

$$C_k' = \tfrac{C_k}{\omega_c} \tag{2.14}$$

Combining both impedance and frequency scaling gives rise to the following equations:

$$L_k' = \tfrac{R_0 L_k}{\omega_c} \tag{2.15}$$

$$C_k' = \tfrac{C_k}{R_0 \omega_c} \tag{2.16}$$

Low-pass filter designs can be transformed to have the bandstop responses. A bandstop response can be obtained by using the transformation $\omega = \Delta(\tfrac{\omega}{\omega_0} - \tfrac{\omega_0}{\omega})^{-1}$ where the fractional bandwidth of the passband is represented by Δ. The center frequency is represented by ω_0. The series inductors of the low-pass prototype are converted to parallel LC circuits having element values given by:

$$L_k' = \tfrac{\Delta L_k}{\omega_0} \tag{2.17}$$

$$C_k' = \frac{1}{\omega_0 \Delta L_k}$$ (2.18)

Similarly, the shunt capacitor of the low-pass prototype is converted to a series LC circuit having the element values:

$$L_k' = \frac{1}{\omega_0 \Delta C_k}$$ (2.19)

$$C_k' = \frac{\Delta C_k}{\omega_0}$$ (2.20)

The lumped elements, namely inductors and capacitors, are difficult to implement at microwave frequencies and have to be approximated with distributed elements. The coupling between the filter components becomes critical at microwave frequencies. The lumped elements are converted to transmission line sections by using Richard's transformation [5], [6]. Further, the filter elements can be separated by using Kuroda's identities [5], [6]. This method of design is the so-called redundant filter synthesis as the additional transmission lines do not affect the filter response. Richard's transformation is given by the equation (2.21)

$$\Omega = \tan \beta l = \tan(\frac{\omega l}{v_p})$$ (2.21)

Where β is the propagation constant, l is the length of the transmission line, ω is the angular frequency and v_p is the propagation constant.

This maps the ω plane to the Ω plane, with a period of $\omega l / v_p = 2\Pi$. Here, the frequency variable ω is replaced with Ω. The reactance of an inductor can be written as

$$jX_L = j\Omega L = jL \tan \beta l$$ (2.22)

The susceptance of a capacitor can be written as

$$jB_C = j\Omega C = jC \tan \beta l \tag{2.23}$$

Thus, an inductor can be replaced with a short-circuited stub of length βl and characteristic impedance L. On the other hand, a capacitor is replaced with an open-circuited stub of length βl and characteristic impedance of 1/C. Since the cutoff occurs at unity frequency for a low-pass filter prototype, the condition to obtain the same cutoff frequency for the Richard's transformed filter gives $\Omega = 1 = \tan \beta l$. This gives a stub length of l=λ/8, λ being the wavelength of the line at the cutoff frequency ω_c. The lines are λ/4 long at a frequency of ω_0=$2\omega_c$ and this results in an attenuation pole. The impedance of the stubs will not match the original lumped element impedances at frequencies far greater than ω_c. The response is periodic in frequency, repeating every $4\omega_c$. Fig. 2.8 shows the Richard's transformations
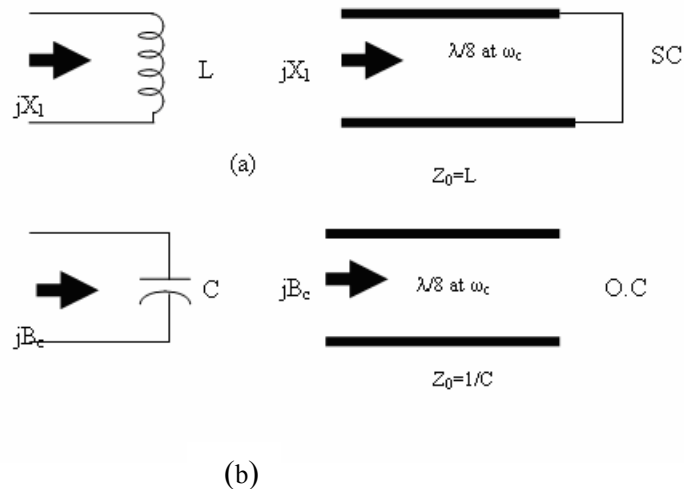
Fig. 2.8 Richard's transformations a) Inductor to a short-circuited stub b) Capacitor to an open-circuited stub

Kuroda's identities [5]-[8] perform the operations of physically separating the transmission line stubs, transforming the series stubs into shunt stubs and vice versa. They also help to change impractical characteristic impedances into more reliable values. The additional transmission line sections used are called unit elements and are λ/8 long at ω_c.

The procedure for designing the stub-loaded lowpass and bandstop filters is summarized in the flowchart shown below in Fig. 2.9.
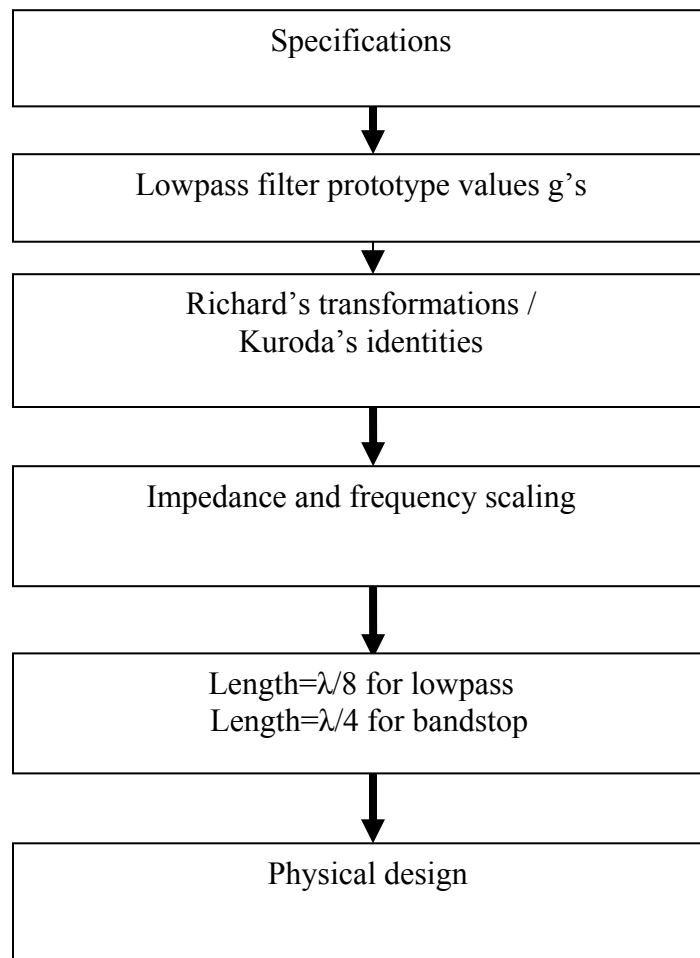
Fig. 2.9 Design flow for the stub-loaded filter design

SINGLE LEVEL FOLDED LINE BANDSTOP AND LOWPASS FILTERS

3.1 Introduction

As explained in section 1.3, the filter sections of the conventional stub loaded bandstop and lowpass filters can be replaced by folded line filter sections. The conventional stub loaded filters at lower RF/microwave frequencies (1-10) GHz, suffer from the disadvantages of large component footprints as the wavelength, λ is large at these frequencies. Additionally, the characteristic impedances of the filter sections are either very large or very small resulting in unrealizable line widths for implementation on a microstrip platform.

In this chapter, it will be demonstrated that the folded line filters on a microstrip platform can have the distinct advantage of reduced overall footprint. In addition, it will also be shown that the transmission line widths will have realizable dimensions for easier implementation on a microstrip platform [15] - [19]. This is demonstrated with the help of several design examples in the following sections.

3.2 Theory

A folded line geometry can be modeled in terms of a set of N-coupled transmission lines. A folded line can be formed by selectively interconnecting the ports of an N-coupled line system as per the requirement of the filter

section. The admittance matrix of an N-coupled line system, which represents a 2N × 2N port network, can be expressed as [20] - [22].

$$[Y] = \begin{bmatrix} Y_A & Y_B \\ Y_B & Y_A \end{bmatrix}$$

(3.1)

where

$$[Y_A] = [M_v]^T [\coth(\gamma_k l)]_{diag} [Y_k]_{diag} [M_v]^{-1}$$

(3.2)

$$[Y_B] = [M_v]^T [\operatorname{csch}(\gamma_k l)]_{diag} [Y_k]_{diag} [M_v]^{-1}$$

(3.3)

$$[Y_k] \approx [M_v]^{-1} [Y_{SH}][M_v]$$

(3.4)

$$[Y_{SH}] = [G] + j\omega[C] \; ; [Z_S] = [R] + j\omega[L]$$

(3.5)

where, [R],[L],[G],[C] are the resistance, inductance, conductance and capacitance matrices of the N-coupled line structure, ω is the angular frequency, [M_v] represents the complex voltage eigenvector matrix associated with the characteristic matrix [Z_S][Y_{SH}], l is the length of the coupled line structure and γ_k is the propagation constant of the kth mode. The network representation shown in Fig. 3.1a consists of N-coupled transmission lines, considered as a 2N-port network with interconnected ports. The folds with the tee-junctions and the small interconnecting lengths of the transmission lines are treated as sub-networks shown as a part of Fig. 3.1b, whose scattering parameters can be easily determined. The reduced 2-port scattering matrix of the folded line filter structure can be derived by selectively eliminating the

unknown incident and reflected amplitudes at the connected ports and relating

the incident and reflected amplitudes of the input and output ports. Based on

the number of filter sections, the order of coupling, N can vary and by using

the network theory described above, a reduced 2-port scattering matrix of the

overall filter can be obtained from the equivalent network representation

shown in Fig. 3.1a.
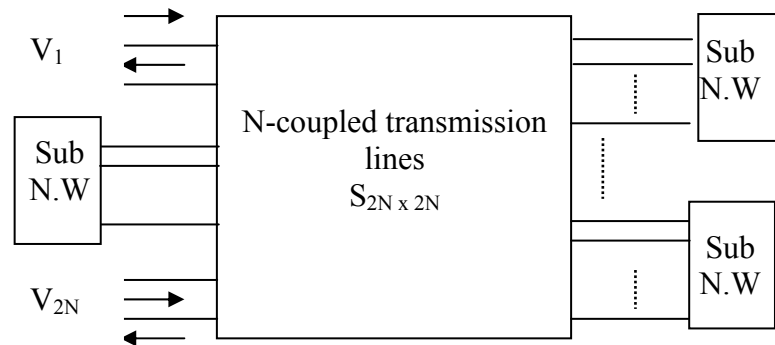
(a)
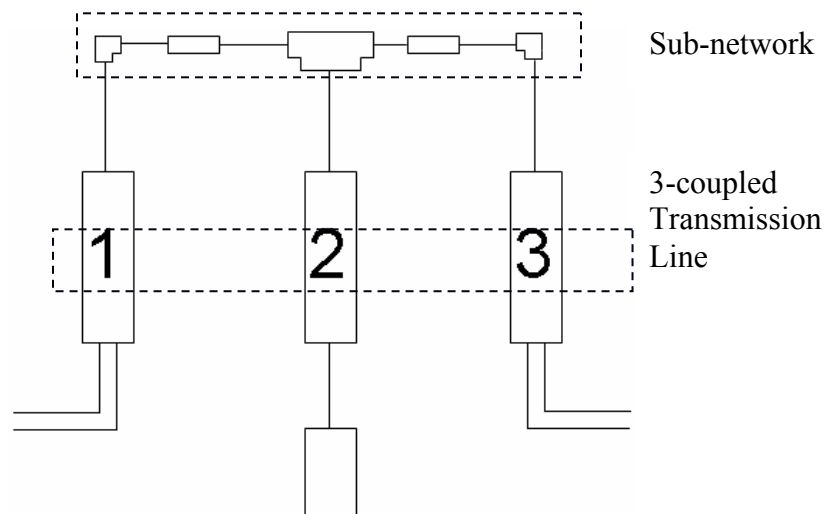
(b)

Fig. 3.1 a) Network representation of an N-coupled line structure
b) Folded line filter section (N=3)

3.3 Design Procedure

One of the main advantages of the folded line design procedure explained here is the use of the conventional stub-loaded filter theory in the first phase of the design. For a given set of specifications for the bandstop/lowpass filters in terms of number of sections N, type of filter (maximally-flat or Chebyshev), center frequency/ bandwidth/ cut-off frequency etc., first the characteristic impedances of various sections for the corresponding shunt-stub design [5] -[8] are calculated in terms of the low-pass filter prototype values, g_i, i=0,1,2….

Next, the filter is divided into N T-sections and each T-section is transformed into an E-section formed by a three-coupled line as shown in Fig. 3.1b. To be able to vary the length of the center stub of the E-section without changing the transmission line lengths, small, variable lengths of transmission line sections are added to the shunt stubs of the folded line design. Interconnecting lengths, corners and additional center stub length are included in the calculations while computing the reduced two-port network parameters of the folded line E-section. The physical parameters of each E-section can be determined by comparing the reduced two-port admittance matrix with that of the corresponding T-section using the procedure explained in the previous section. This can establish a relation between the network parameters of the E-section and the lowpass prototype values, g_i, i=0,1,2.... The physical parameters of each E-section are optimized to provide the closest values for g_i and

electrical lengths for a given set of specifications. The other distinct advantage of this procedure is its applicability for both bandstop and lowpass designs as both designs can be realized in the conventional shunt-stub loaded configurations. This is explained with the help of several examples in the following section.

3.4   Results and Discussion

3.4.1 Folded line bandstop filters

To demonstrate the design feasibility of the new design procedure explained in the earlier section, initially, a 3-section folded line bandstop filter was designed for a maximally flat response at a center frequency of 1.5 GHz and a fractional bandwidth, $\Delta = 0.3$. The first phase of the design involves the modeling of a 3-section conventional stub-loaded bandstop filter. The procedure was already explained using the flow-graph in Fig. 2.9. The design equations for the 3-section stub loaded bandstop filter [6]-[7] are summarized in equations 3.2-3.10.

Here Z_A and Z_B represent the terminating impedances (50 Ω lines), Z_j (j=1 to n) are the open circuit shunt stub impedances, Zij (j=1 to n) are the interconnecting line impedances, g_j(j=0 to n) are the low-pass prototype element values and ω_1 and ω_2 are the bandstop edge frequencies. A generic layout for the conventional stub-loaded bandstop filter is shown in Fig. 3.2. Here all the transmission lines are of length $\lambda/4$.

$$Z_1 = Z_A \left(1 + \frac{1}{\Lambda g_0 g_1}\right) \tag{3.2}$$

$$Z_{12} = Z_A \left(1 + \Lambda g_0 g_1\right) \tag{3.3}$$

$$Z_2 = Z_A \frac{g_0}{\Lambda g_2} \tag{3.4}$$

$$Z_3 = Z_A \frac{g_0}{g_4} \left(1 + \frac{1}{\Lambda g_3 g_4}\right) \tag{3.5}$$

$$Z_{23} = Z_A \frac{g_0}{g_4} \left(1 + \Lambda g_0 g_1\right) \tag{3.6}$$

$$\Lambda = \omega_c a \tag{3.7}$$

$$a = \cot\left(\frac{\pi}{2} \frac{\omega_1}{\omega_c}\right) \tag{3.8}$$

$$\Delta = \frac{\omega_2 - \omega_1}{\omega_c} \tag{3.9}$$

$$\omega_c = \frac{\omega_1 + \omega_2}{2} \tag{3.10}$$
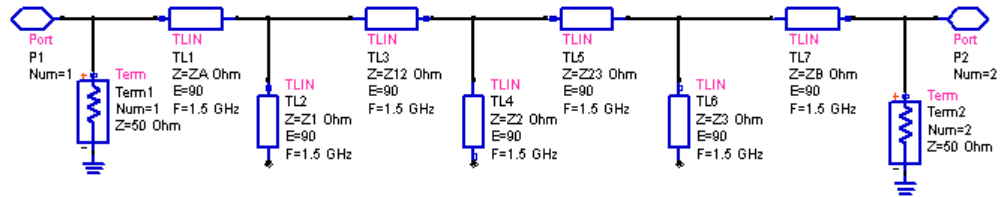
Fig. 3.2 Generic layout for the conventional stub-loaded bandstop filter

Using the equations (3.2-3.10), we can obtain the characteristic impedance values for the various bandstop filter sections. The corresponding impedance values for this filter design ($\Delta=0.3$) are provided in Table 3.1. All the transmission lines are of length $\lambda/4$ for this stub-loaded bandstop filter.

Δ	Z_A (Ω)	Z_1 (Ω)	Z_{12} (Ω)	Z_2 (Ω)	Z_{23} (Ω)	Z_3 (Ω)	Z_B (Ω)
0.3	50	258	62	104	62	258	50
0.2	50	365.7	57.9	157.8	57.9	365.7	50

Table 3.1 Characteristic impedance values for the various bandstop filter sections (Maximally flat response, f_0=1.5 GHz, Δ=0.3)

The individual sections of this stub-loaded filter are replaced with folded line E-sections as explained in section 3.3. Each section of the folded line bandstop filter is optimized separately to match the response of the corresponding section of the conventional stub-loaded filter. The Random/Quasi-Newton optimizer combination is employed for this purpose and required the use of Agilent EDA software [24]. The optimization band was 0.5-2.5 GHz with the center frequency of the bandstop filter being 1.5 GHz. The folded line filter was constructed by combining all three E-sections. The design parameters for the individual optimization of each E-section are the widths w_1, w_2, w_3 of the three coupled lines, the spacings between the coupled lines s_1, s2, and the lengths of the coupled lines. Additionally thin transmission lines were added to the open-circuit shunt stubs of the first and third sections of the filter. The width w_0 and length of this line were also included as the design parameters for the optimization of the individual filter sections. The design flow for the folded line bandstop filter is summarized in Fig. 3.3.

(a)

(b)

(c)

Section 1   Section 2   Section 3

(d)

Section 1   Section 2   Section 3
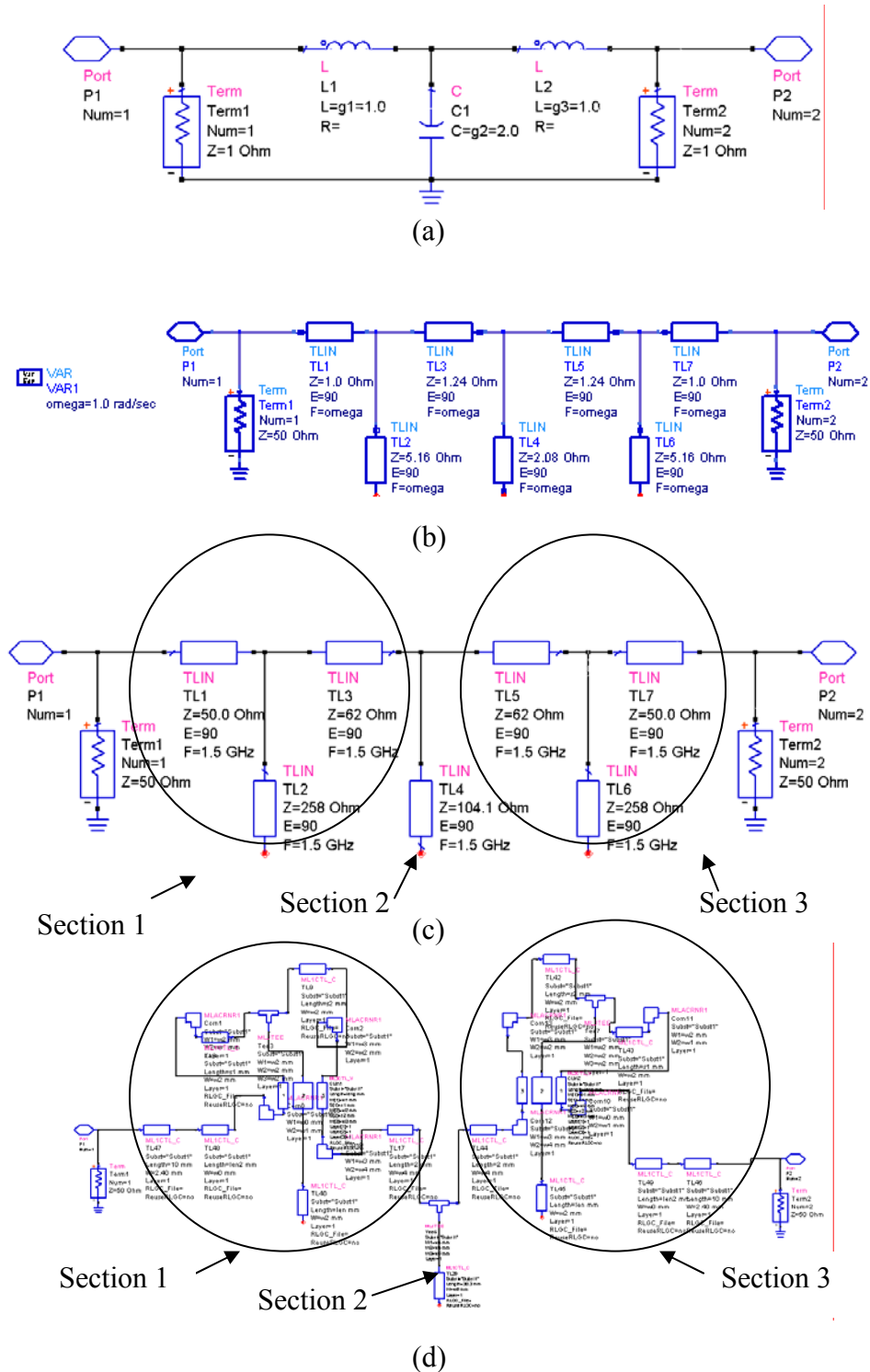
Fig. 3.3 Design flow for the folded line bandstop filter (f_0=1.5 GHz, Δ=0.3) (a) Lumped-element low-pass prototype (b) Richard's transformations/ Kuroda's identities (c) Conventional stub-loaded filter after impedance and frequency scaling (d) Folded line filter

The individual responses of each folded line filter section, optimized with reference to the corresponding section of the conventional stub-loaded bandstop filter are shown in Fig. 3.4. The folded line filter sections were implemented on a microstrip platform with ε_r=2.2 and a substrate height h=31 mil. Section 3 is essentially the same as section 1 with the port locations interchanged. By cascading these folded line filter sections, the overall response of the folded line bandstop filter can be obtained.

The disadvantage of the conventional stub-loaded bandstop filter lies in the fact that transmission lines with impedances of the order of 258 Ω would have a line width of about 1 mil, which makes it impossible for a physical realization. Fig. 3.5 shows the layouts for the designed 3-section folded line bandstop and the conventional stub-loaded filter designs. Sections 1 and 2 are shown in Fig. 3.5. Section 3 is the same as section 1 and is not shown. The corresponding physical dimensions are shown in Table 3.2. The line widths of the OC shunt stubs of the first and third sections of the conventional bandstop filter are very small (0.02 mm); hence the layout comparison as shown in Fig. 3.5 is not to scale. The overall footprint in the case of the folded line bandstop filter is only 34 % of the overall footprint of the conventional design. Table 3.3 gives a comparison of the smallest normalized width (w/h) of the conventional design and the folded-line design. It can be seen that the normalized conductor widths for the new folded design are much larger (0.5 versus 0.032). This

allows practical realization of the folded line filter with less stringent dimensional tolerances thus facilitating a relatively easy fabrication.
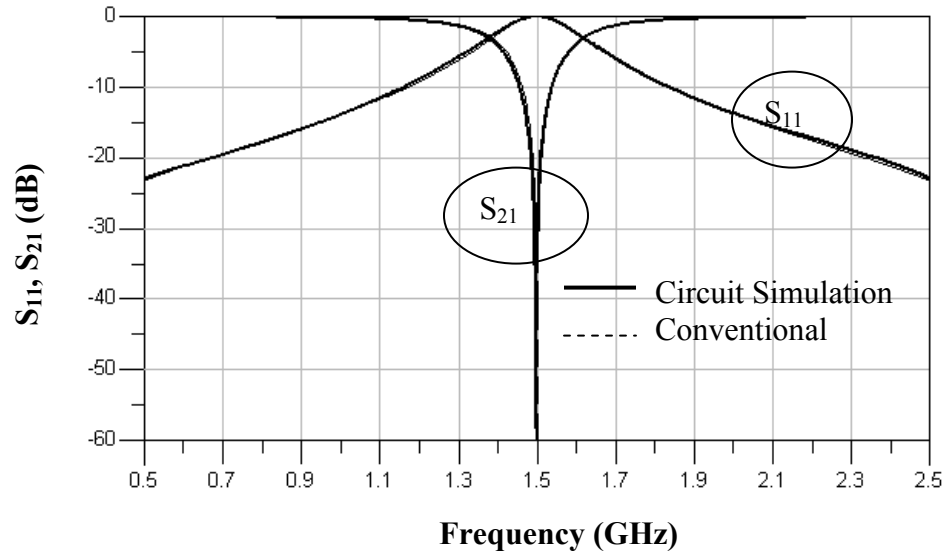
(a)
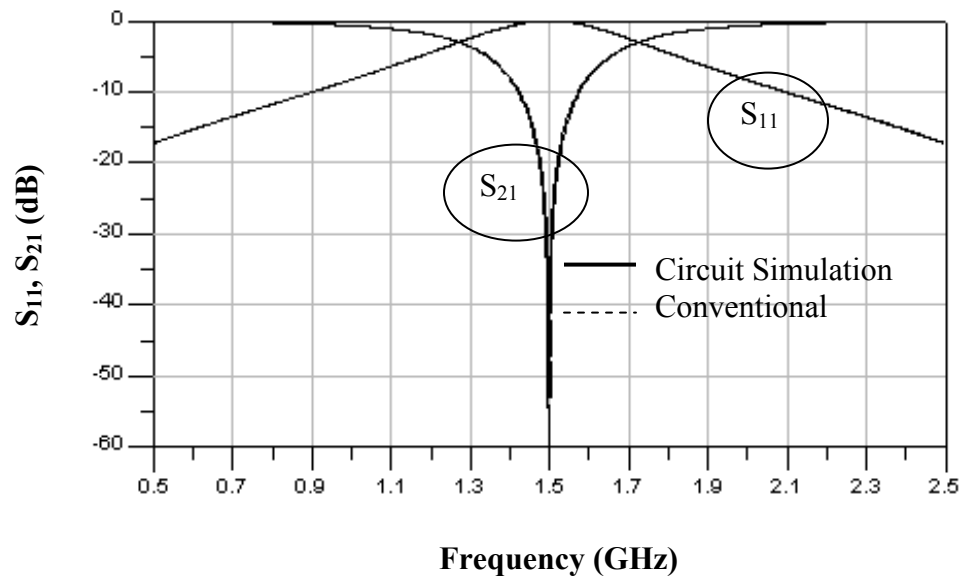
(b)

Fig. 3.4 Optimization results for the folded line bandstop filter sections (Δ=0.3) (a) Section 1 response comparison (b) Section 2 response comparison
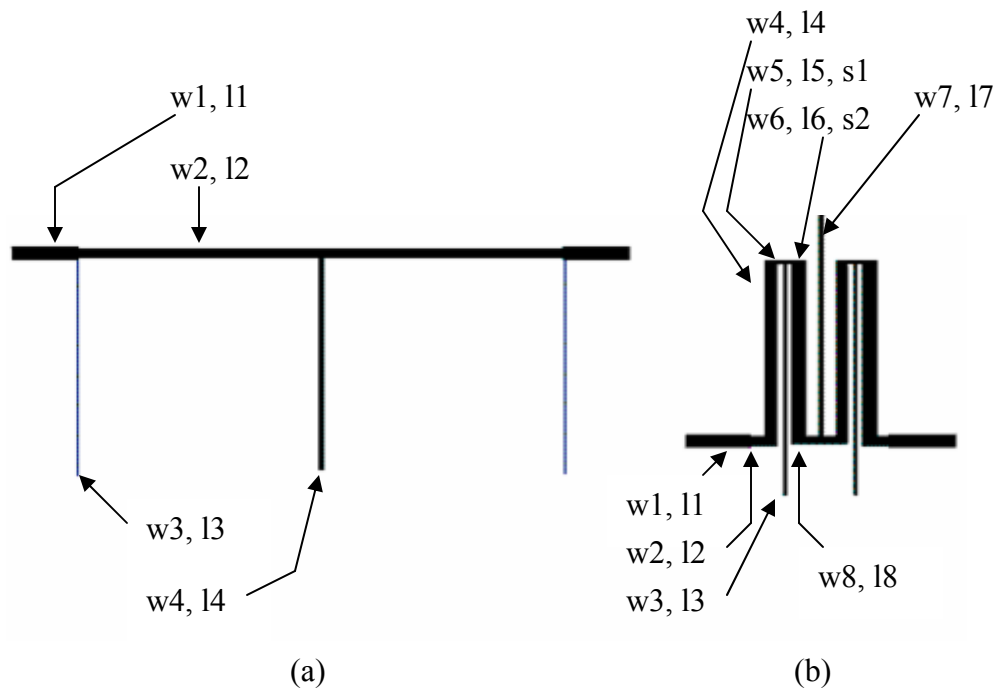
**Fig. 3.5 Physical layout comparison for the bandstop filter (Δ=0.3)
(a) Conventional stub-loaded filter (b) New folded line design**

Parameter	Conventional Bandstop	Folded Line Bandstop
Width(mm)	w1=2.4 ; w2=1.7 w3=0.02; w4=0.6	w1=2.4; w2=1.7; w3=0.4; w4=2.3; w5=0.4; w6=1.6; w7=0.6; w8=1.4
Length(mm)	l1=10; l2=36.7 l3=38.7; l4=37.6	l1=10.0; l2=2.0; l3=10.0; l4=29.9; l5=29.9; l6=29.9; l7=38.3; l8=2.0
Spacing(mm)	NA	s1=0.6; s2=1.0

Table 3.2 Physical dimensions for the conventional stub-loaded bandstop filter and the new folded line design (Δ=0.3)

Δ=0.3	Conventional Bandstop	Folded line Bandstop
Smallest normalized width (w/h)	0.032	0.5
Overall footprint	2948.2 sq mm	1015.1 sq mm
Footprint comparison	100 %	34 %

Table 3.3 Footprint and critical conductor width comparison for the single-level folded line bandstop filter (Δ=0.3).

full-wave EM simulation using CST Microwave Studio® [23] and Agilent Momentum [24] for the folded line bandstop filter. A time-domain solver was used in the case of CST Microwave Studio® and a frequency domain solver in the case of Agilent Momentum. In general, there is a good agreement in the insertion loss response. A slight deterioration in the return loss characteristics is noticed in the upper pass band and this can be attributed to the mutual coupling between the filter sections of the folded line bandstop filter which was only taken into account in the full wave EM simulation. The mutual coupling between the filter sections plays a predominant role in the design of the folded transmission line filters and it increases as the frequency range is increased.
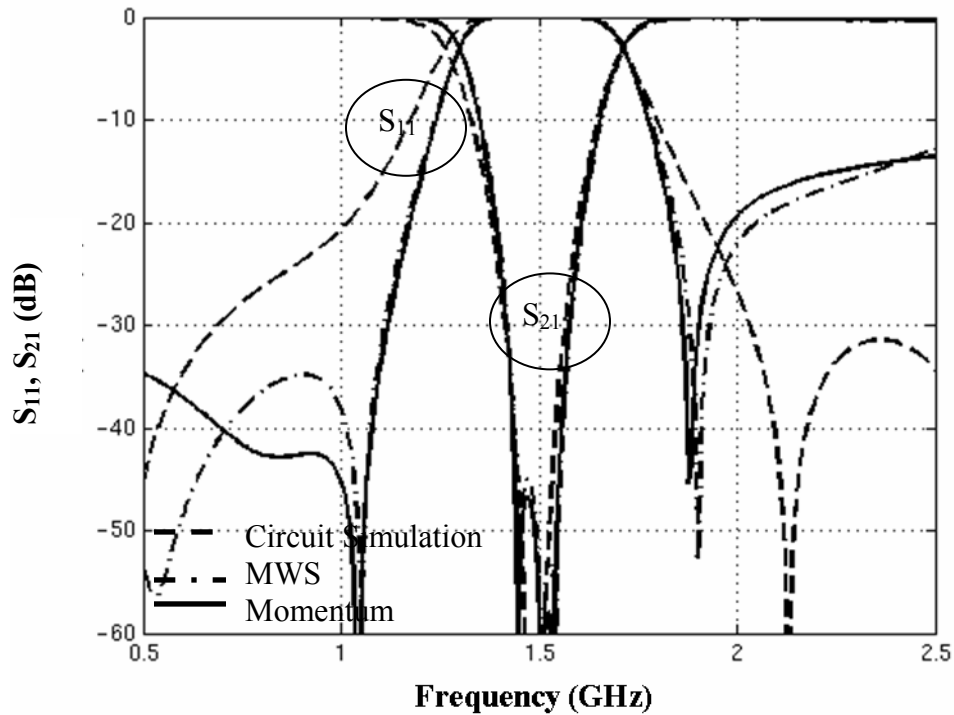
Fig. 3.6 Folded line bandstop filter response (f$_0$=1.5 GHz, Δ=0.3)

To further validate this new methodology for designing folded line filters, a folded line bandstop filter was designed for a maximally flat response at a center frequency of 1.5 GHz and a fractional bandwidth, Δ=0.2. The design procedure is the same as that explained above. The first step involves the design of the conventional stub-loaded filter. The characteristic impedance values of the transmission lines for the conventional filter are shown in Table 3.1. Impedances of the order of 365 Ω would have a line width of 0.1 mil, which makes it impossible for practical implementation. This folded line filter was implemented on a microstrip platform with ε$_r$=2.2 and a substrate height h=31 mil.
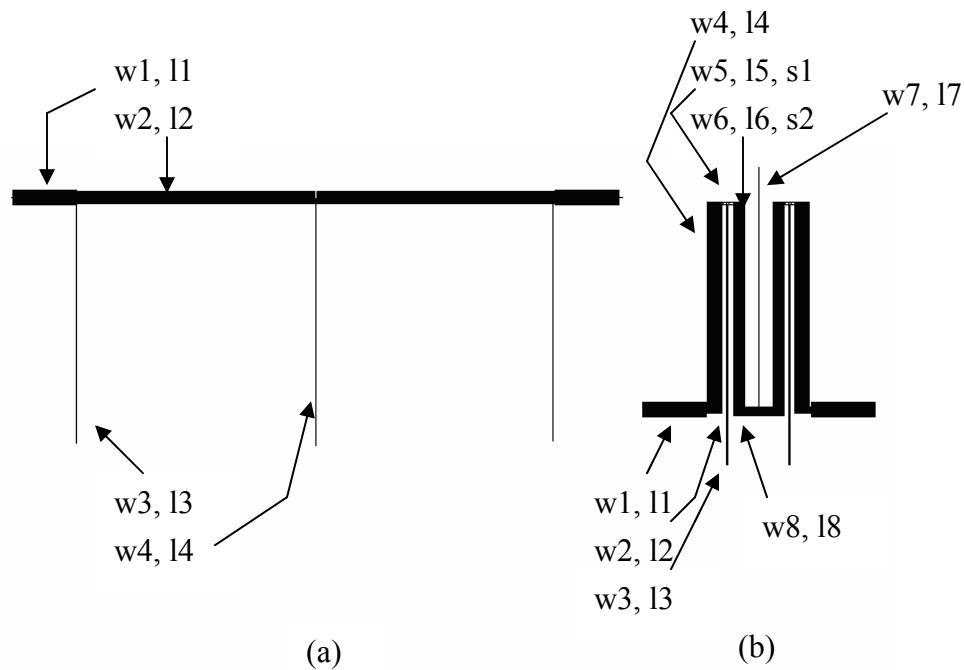
Fig. 3.7 Physical layout comparison for the bandstop filter (Δ=0.2)
(a) Conventional stub loaded filter (b) New folded line design

Parameter	Conventional Bandstop	Folded Line Bandstop

Width(mm)	w1=2.4 ; w2=1.9
	w3=0.002; w4=0.2
		w1=2.4; w2=1.0; w3=0.3;
		w4=2.3; w5=0.3; w6=1.8;
		w7=0.3; w8=1.4

Length(mm)	l1=10; l2=36.6
	l3=38.9; l4=38.2
		l1=10.0; l2=0.07; l3=9.0;
		l4=31.1; l5=31.1; l6=31.1;
		l7=38.3; l8=2.0

Spacing(mm)	NA	s1—0.6; s2—0.6

Table 3.4 Physical dimensions for the conventional stub-loaded bandstop filter and the new folded line design (Δ=0.2)

The physical layout comparison of the folded line bandstop filter and

its conventional counterpart is shown in Fig. 3.7. Sections 1 and 2 are shown in

Fig. 3.7. Section 3 is the same as section 1 and is not shown. The line widths of the OC shunt stubs of the first and third sections of the conventional bandstop filter are very small (0.002 mm); hence the layout comparison as shown in Fig. 3.7 is not to scale. The physical dimensions of the corresponding designs are shown in Table 3.4. The overall footprint in the case of the folded line bandstop filter is only 26 % of the overall footprint of the conventional design. Table 3.5 gives a comparison of the smallest normalized width (w/h) of the conventional design and the stub-loaded design. It can be seen that the normalized conductor widths of the folded line design are much larger (0.26 versus 0.0032). This allows a physical realization of the folded line filter with less stringent dimensional tolerances. Fig. 3.8 shows the circuit simulation results of the folded line filter as well as the conventional stub- loaded filter using Agilent EDA software [24]. These results are further validated in the case of the folded line design by using full wave EM simulation using Agilent Momentum [24]. Once again there is a good agreement in the insertion loss response, the return loss in the lower and upper passbands being lesser than -20 dB. The slight deterioration in the results can be attributed to the mutual coupling between the folded line filter sections, which was only considered in the case of full wave EM simulation. The mutual coupling between the filter sections increases with the increase in the frequency range.

Δ=0.2	Conventional Bandstop	Folded line Bandstop
Smallest normalized width (w/h)	0.0032	0.26
Overall footprint	2946.2 sq mm	766.5 sq mm
Footprint comparison	100 %	26 %

Table 3.5 Footprint and critical conductor width comparison for the single-level folded line bandstop filter (Δ=0.2)
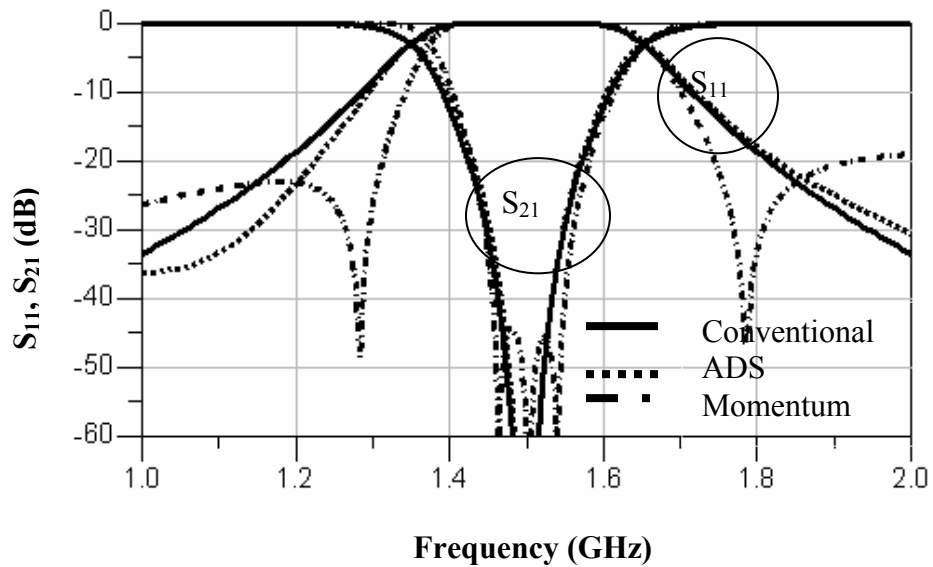
Fig.3.8 Folded line bandstop filter response (f$_0$=1.5 GHz, Δ=0.2)

3.4.2 Folded line lowpass filters

A 3-section lowpass filter was designed for a maximally flat response with a cut-off frequency of 1.5 GHz, and with the substrate specifications remaining the same as mentioned above. The conventional stub-loaded filter

can be derived starting with the lowpass prototype values g_i, i=0,1,2… and following the procedure described in the flow graph in Fig. 2.9. The lengths of the transmission lines are $\lambda/8$ in the case of the stub-loaded lowpass filter. The characteristic impedance values of the lowpass filter sections of the conventional stub-loaded filter are provided in Table 3.6. From the conventional stub-loaded filter, the design procedure for the folded line lowpass filter is similar to that of the folded line bandstop filter explained earlier in *3.4.1*.

	Z_A Ω	Z_1 Ω	Z_{12} Ω	Z_2 Ω	Z_{23} Ω	Z_2 Ω	Z_B Ω
ω_c=1.5 GHz	50	100	100	25	100	100	50

Table 3.6 Characteristic impedance values for the various lowpass filter sections (Maximally flat response, f_c=1.5 GHz).

Thus, the physical dimensions of the folded line lowpass filter are obtained by optimizing each section of the folded line filter to match the response of the corresponding section of the conventional lowpass filter. The Random/Quasi-Newton optimizer combination is employed for this purpose and required the use of Agilent EDA software [24]. The optimization band was 0.5-2.5 GHz with the cut-off frequency of the lowpass filter being 1.5 GHz. The central stub of the conventional lowpass filter has a characteristic impedance of 25 ohms. Fig. 3.9 shows the design flow for the folded line filter.
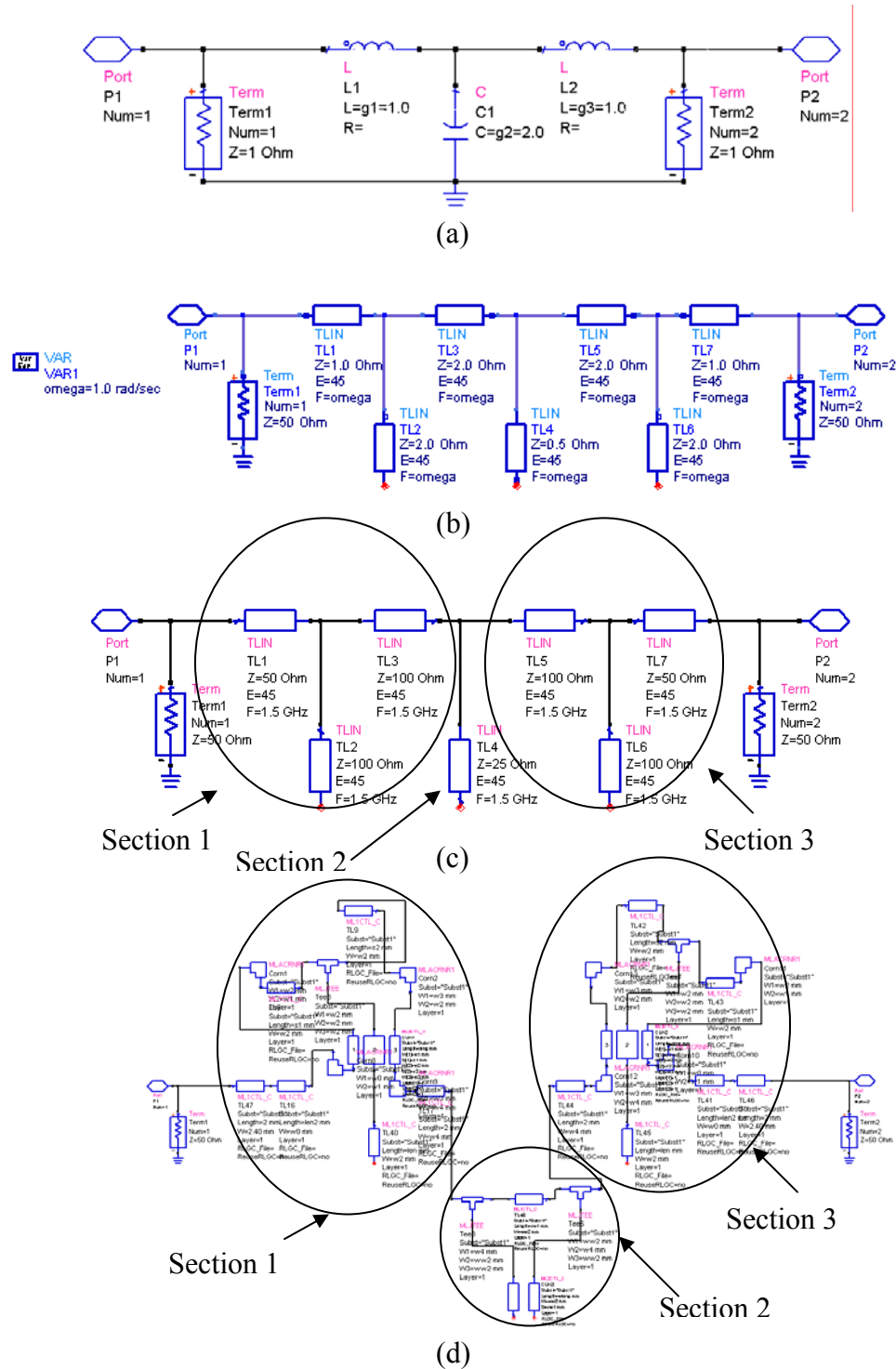
Fig. 3.9 Design flow for the folded line lowpass filter response (f_c=1.5 GHz) (a) Lumped-element low-pass prototype (b) Richard's transformations/ Kuroda's identities (c) Conventional stub-loaded filter after impedance and frequency scaling (d) Folded line filter

When the conventional filter is implemented on a microstrip platform with ε_r=2.2 and substrate height h=31 mil, this stub is extremely wide (w/b ~8). This has been replaced by two parallel coupled stubs shown as section 2 in Fig. 3.9 (d) in the case of the folded line lowpass filter. The widths and central spacing of the parallel-coupled stubs were optimized to provide a close match in response with that of the single stub, shown as section 2 in Fig. 3.9 (c). Fig 3.10 shows the optimization results for Sections 1 and 2 of the folded line filter. Section 3 is the same as Section 1 and it has not been shown in Fig. 3.10. The footprint comparison of the folded line configuration and the conventional lowpass filter is shown in Fig. 3.11. Sections 1 and 2 are shown in Fig. 3.11. Section 3 is the same as section 1 and is not shown. The layouts as shown in Fig. 3.11 are to scale. The physical dimensions of the corresponding designs are shown in Table 3.7. The overall footprint of the folded line lowpass filter is only 71% of the overall footprint of the conventional filter. Table 3.8 gives a comparison of the largest normalized width (w/h) of the conventional design and the folded-line design. From Table 3.8, it can be seen that the normalized conductor widths for the new folded line lowpass design are much smaller (3.63 versus 7.9). Fig. 3.12 shows the theoretical results in comparison with the full wave EM simulation using CST Microwave Studio® [23] and Agilent Momentum [24] for the folded line lowpass filter. A time domain solver was used in the case of CST Microwave Studio® and a frequency domain solver in

the case of Agilent Momentum. The insertion loss and return loss responses

show good agreement between theory and full wave EM simulation.
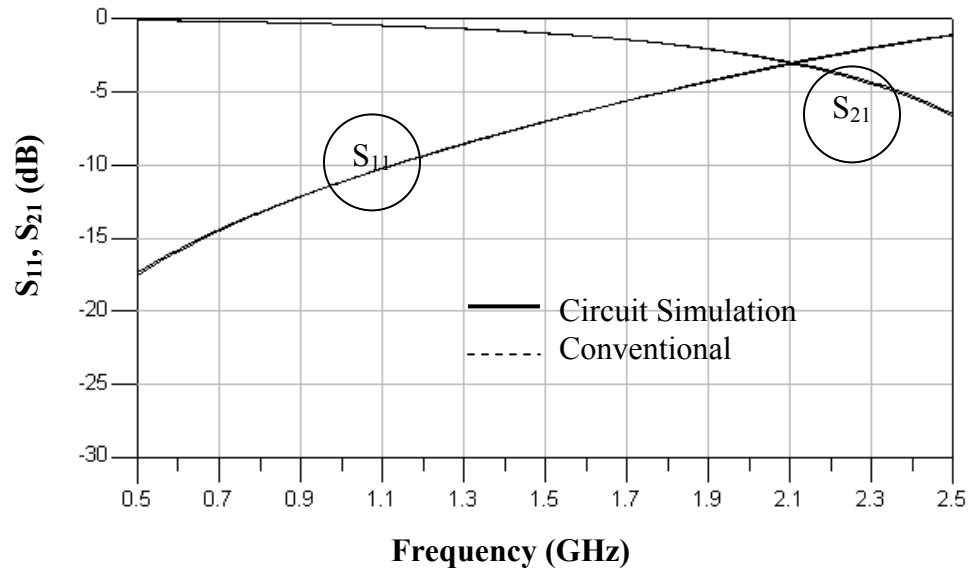
(a)
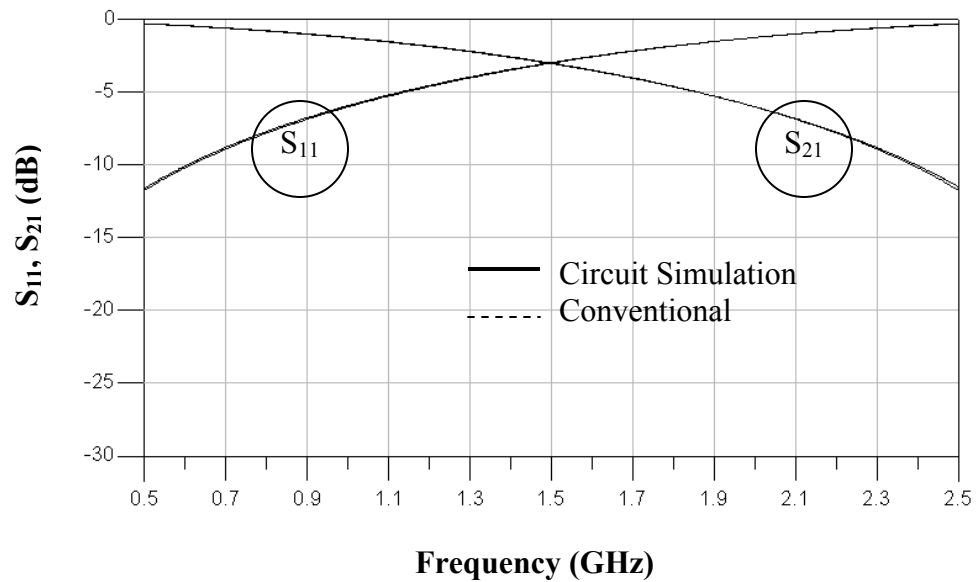
(b)

Fig. 3.10 Optimization results for the folded line lowpass filter sections (f$_c$=1.5 GHz) (a) Section 1 response comparison (b) Section 2 response comparison
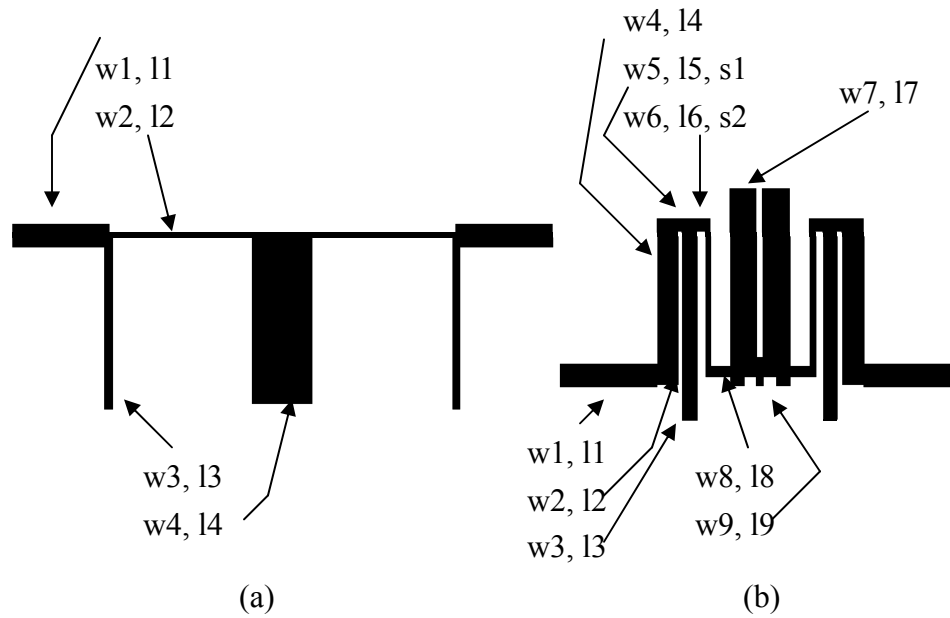
Fig. 3.11 Physical layout comparison for the lowpass filter (f_c=1.5 GHz) (a) Conventional stub-loaded filter (b) New folded line design

Parameter	Conventional Lowpass	Folded Line Lowpass		
Width(mm)	w1=2.4 ; w2=0.7 w3=0.7; w4=6.1	w1=2.4; w2=1.7; w3=1.2;		
		w4=2.1; w5=1.3; w6=0.5;		
		w7=2.8; w8=1.0; w9=2.8		
Length(mm)	l1=10; l2=18.2 l3=18.2; l4=17.6	l1=10.0; l2=0.07; l3=5.7;		
		l4=14.2; l5=14.2; l6=14.2;		
		l7=17.8; l8=2.0; l9=0.6		
Spacing(mm)	NA	s1=0.5; s2=1.0		

Table 3.7 Physical dimensions for the conventional stub-loaded lowpass filter and the new folded line design (f_c=1.5 GHz)

f_c=1.5 GHz	CONVENTIONAL LOWPASS	FOLDED LINE LOWPASS
Largest normalized width (w/h)	7.9	3.63
Overall footprint	754.9 sq. mm	534.84 sq. mm
Footprint comparison	100 %	71 %

Table 3.8 Footprint and critical conductor width comparison for the single-level folded line lowpass filter
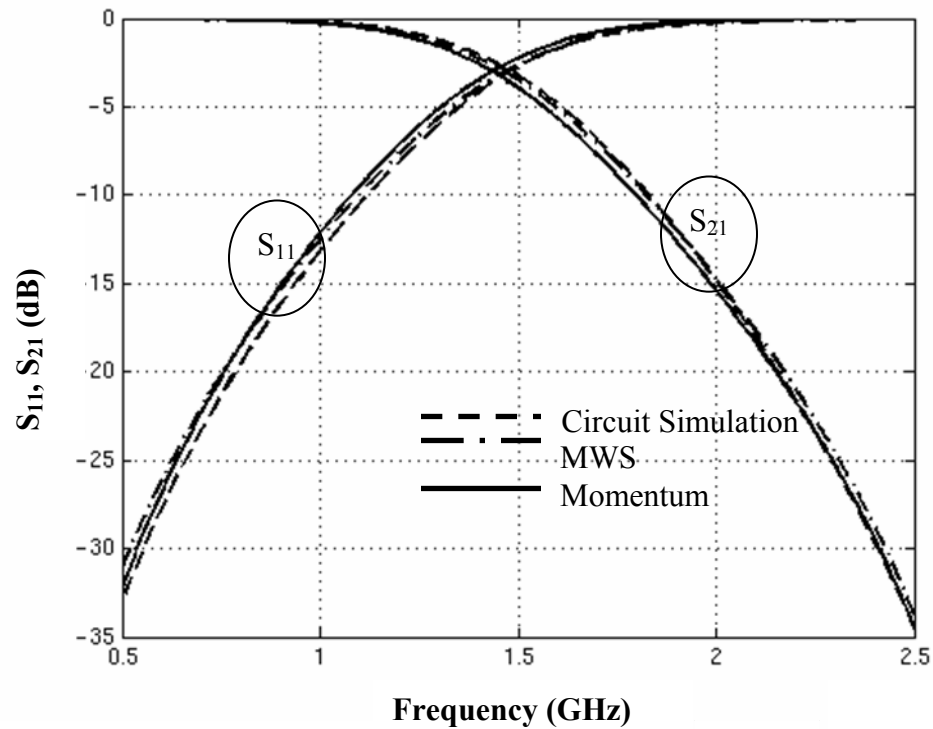
Fig. 3.12 Folded line lowpass filter response (f_c=1.5 GHz)

4. MULTI-LEVEL BANDSTOP AND LOWPASS FILTERS ON BACK-TO-BACK MICROSTRIP

4.1   Introduction

As explained in chapter 3, folding the transmission lines on a single-level geometry can lead to compact footprint. Further compactness can be achieved by folding the transmission lines in a multi-layer, multi-conductor environment [9]-[11] [19] [25] [31]-[33]. The cross-section of a multi-layer transmission line model is shown in Fig. 4.1a. Vias are used to interconnect the top and bottom metallization layers. One of the main problems in this type of geometry is that the broadside coupling between the transmission lines can have a negative influence in the design of multi-level filters. The dielectric layers have to be made especially thick in order to minimize this effect. On the other hand, if the vias are electrically very long they can exhibit more distributed behavior and in certain cases, the EM simulations may not be accurate. Furthermore, the top and bottom metal layers have to be aligned exactly on top of each other and any misalignment would result in an incorrect filter response.

To minimize the associated disadvantages with the multi-level geometry shown in Fig. 4.1a, a back-to-back (BTB) microstrip platform is proposed as shown in Fig 4.1b. Here, the top and bottom dielectric layers are isolated by an intermediate ground plane. This ensures that the top and bottom

metallization layers are sufficiently isolated thus aiding in the design of the multi-level filters.

Through-ground vias can be developed easily using full wave EM simulation to interconnect the metallization layers. The through-ground vias will have realizable physical dimensions. Further, any slight misalignment of the top and bottom metallization layers would not adversely affect the filter response due to the presence of the intermediate ground plane.

(a)

(b)
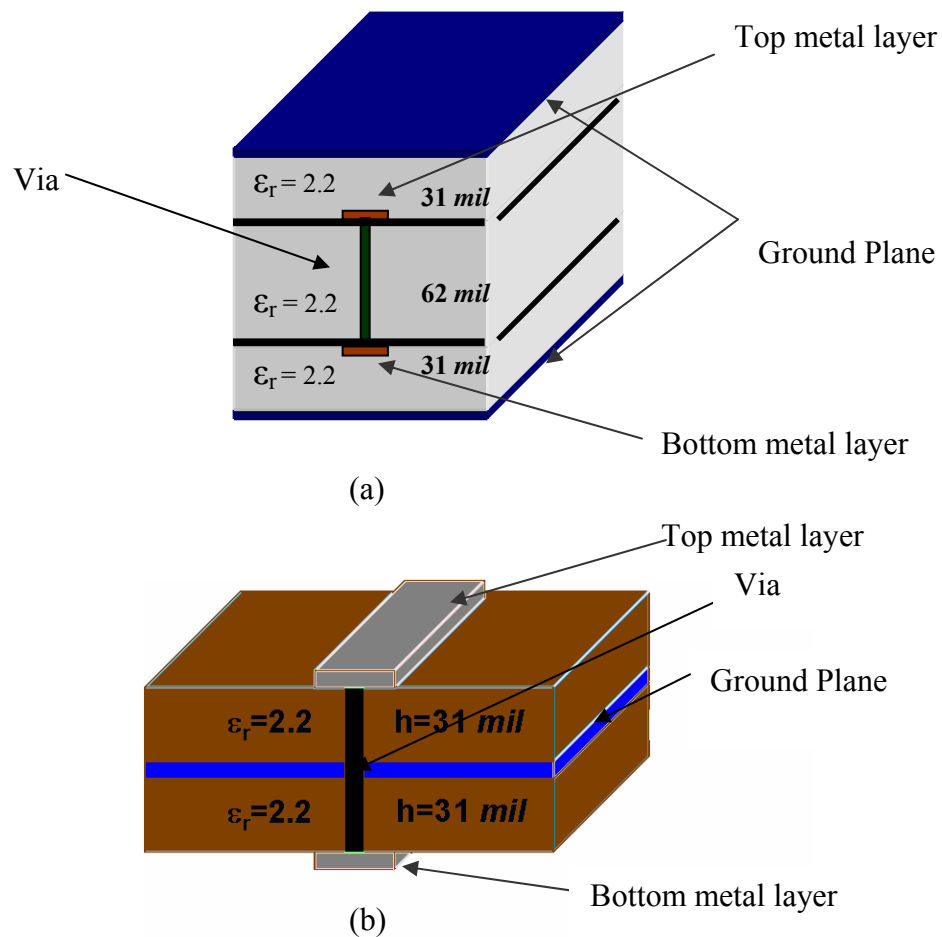
Fig. 4.1 Cross-sectional view of multi-level transmission line models (a) With no intermediate ground plane (b) With an intermediate ground plane (BTB microstrip) geometry.

4.2 Theory

Multi-level folded line geometry can be modeled as a set of N-coupled transmission lines interconnected by vias as shown in Fig. 4.2. An N-coupled line system, which represents a 2N × 2N port network, can be expressed as [20] - [22]. The equation for the admittance matrix for such an N-coupled line system was already shown in equation (3.1). The length l of the N-coupled line system will be much smaller than in the case of a single-level geometry as the transmission lines have now been folded onto different layers.

A reduced two-port scattering matrix of the overall filter can be obtained from the equivalent network representation shown in Fig. 4.2. Analysis of the structure can be carried out by considering the overall structure as a cascade of three separate networks, as shown in Fig 4.2. The coupling between the networks has been taken into account for this analysis.

On a back-to-back microstrip configuration as shown in Fig 4.1b, the top and bottom dielectric layers are isolated by an intermediate ground plane. The two metallization layers shown as top metal layer and bottom metal layers are connected by through-hole vias in the ground plane. This is shown in Fig. 4.3. The top metal layer consists of N-parallel multiple coupled lines which are connected to N-parallel multiple coupled lines on the bottom metal layer through N-through-hole vias as shown in Fig. 4.4. The mutual coupling between the vias is taken into consideration for this analysis. The through-ground via model extraction is explained later in section 4.3.

V_1

Sub N.W

V_{2N}

N-Coupled
Transmission Lines
$S_{2N \times 2N}$

N-Through-ground
Vias

N-Coupled
Transmission Lines
$S_{2N \times 2N}$

Sub N.W

Sub N.W
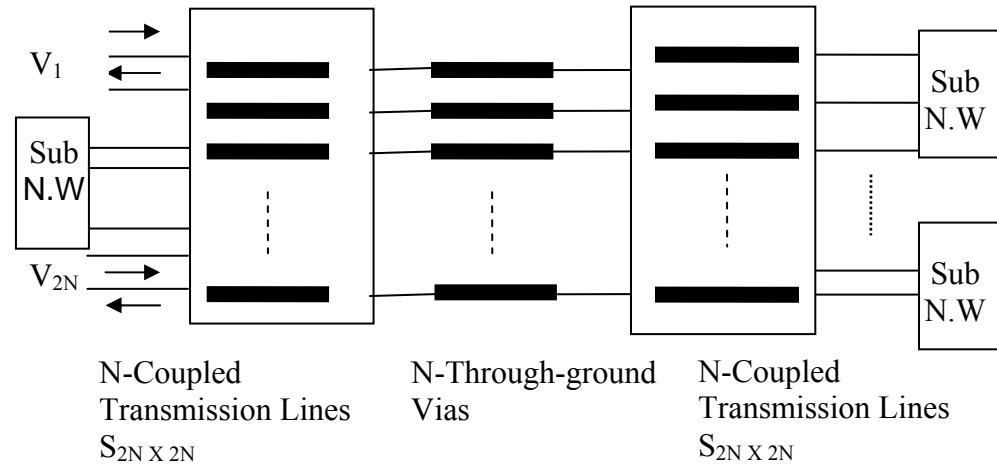
Fig. 4.2 Network representation of a multi-level folded line geometry

Top metal layer

Through-hole vias

Ground Plane
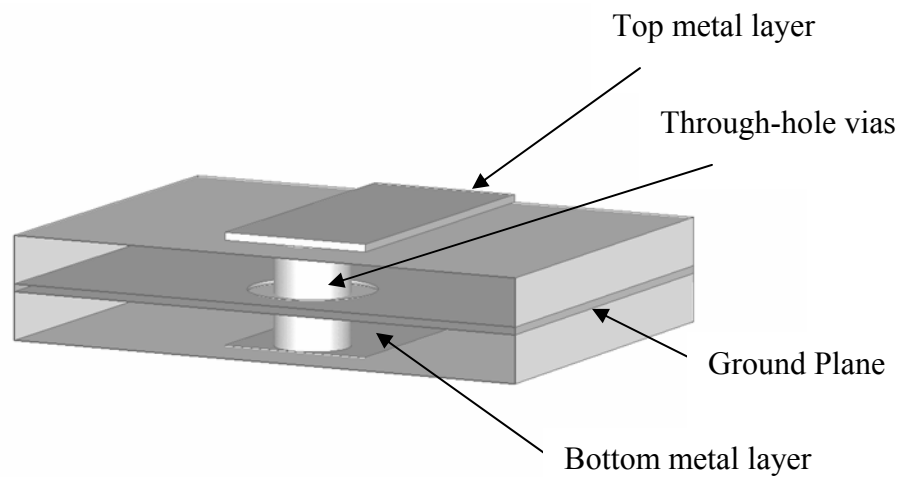
Bottom metal layer

Fig. 4.3 A back-to-back microstrip geometry

Through hole vias

Ground Plane

Top metal layer
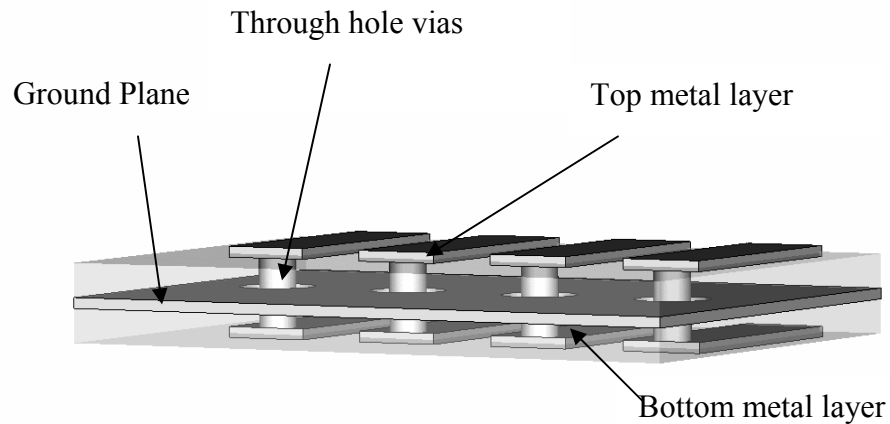
Bottom metal layer

Fig 4.4 Top and bottom metal layers modeled as N multiple coupled transmission lines

The presence of an intermediate ground plane enables the coupled line structures above and below the ground plane to be sufficiently isolated so that they can be modeled as two sets of single-level multiple coupled parallel lines using the available analytical techniques[10] [20]-[22] [26]. The interaction between the various lines in a multiple coupled line system can be modeled in terms of the normal-mode parameters [20] [21], or with the use of the inductance and capacitance matrices of the coupled-line system. Expressions similar to equation (3.1) can be derived for the admittance matrices in terms of the inductance and capacitance matrices for inhomogeneous media like microstrip applications. Once the admittance matrices have been determined for the multiple coupled lines in the top and the bottom layers, the next step is

to obtain a suitable model for the via through a ground plane, which is shown in Fig 4.5a.

4.3   Via model extraction

A lossless model for the through ground via structure was previously reported by Bahl [27], which can be modified to include metallic and dielectric losses. The resulting pi-model for the via through the ground plane is shown in Fig 4.6b. The equivalent circuit parameters of the via model can be extracted from the two-port network parameters of the via structure, which in turn are determined from full wave EM simulations. For a given strip width, substrate thickness and dielectric constant, the extracted model can be used for the realization of a wide range of passive geometries.

The complete network model of the multi-layer folded line filter as shown in Fig. 4.2 can then be analyzed with the top metal layer and bottom metal layers interconnected by the through-ground via equivalent circuit. The through-ground vias are used to interconnect the top and bottom metal layers. The lumped equivalent circuit of the via model is shown in Fig 4.6b where the R, L, C values have been expressed as functions of the line width w in equations (4.2-4.4). Here R refers to the resistance, L the inductance and C the capacitance. The 3D EM model for the via is shown in Fig. 4.5a and the equivalent circuit model is shown in Fig. 4.5b. In Fig. 4.5a the reference planes have been de-embedded to calculate the scattering parameters for the via only.

$$L(w) = 0.5054 * \exp(-1.7014 * w^{0.8846}) + 0.4298 \qquad (4.2)$$

$$C(w) = 0.2209 * \exp(0.2564 * w^{0.9555}) - 0.1918 \qquad (4.3)$$

$$R(w) = -0.0026 * \exp(1.6083 * w^{0.5072}) + 0.0911 \qquad (4.4)$$
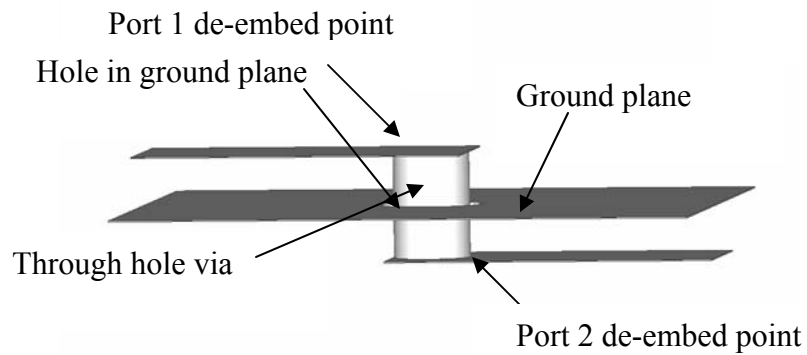
(a)
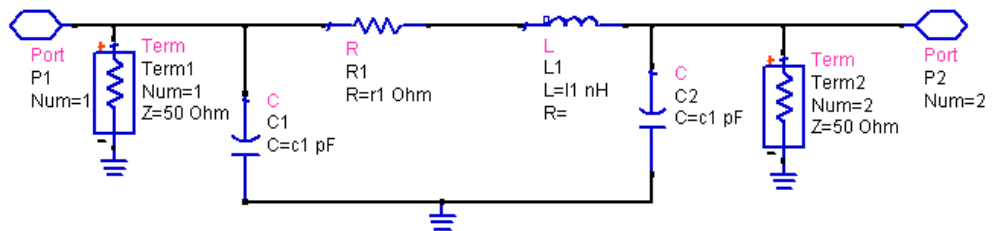
(b)

Fig 4.5 Via through ground plane (a) 3-D view (b) Equivalent circuit

These are derived by a direct comparison of the scattering parameters of the via model as shown in Fig. 4.5a obtained from full wave EM simulation using CST Microwave Studio® [23] with the scattering parameters obtained from the lumped network model for the via as shown in Fig 4.5b. The optimization setup to determine the R, L, C values is shown in Fig 4.6. The via model, the 3-D view of which is shown in Fig 4.5a has been implemented with the diameter of the via chosen as w/2, where w is the line width and the diameter of the hole in the ground plane chosen to be 0.4 mm larger than w/2. The diameter of the hole in the ground plane also known as the antipad diameter has been so chosen to ensure that the via does not touch the ground plane. Further, this optimum value of 0.4 mm ensures that physical realization is possible and the capacitance to the ground is not too large due to the proximity of the ground plane.

The line width w was varied from 0.1 mm to 3.0 mm and for each value of w; the optimization gives a new set of R, L, C values. The Random/Quasi-Newton optimizer combination is employed for this purpose and required the use of Agilent EDA software [24]. The optimization band was 0.5-2.5 GHz. The R, L, C data thus obtained was curve fitted to result in the closed form expressions shown in equations (4.2-4.4). The specific form of closed form expressions as shown in equations (4.2-4.4) was so chosen to minimize the error between the transfer function of the EM-based via model as shown in Fig 4.5a and the transfer function of the network model of the via as

shown in Fig 4.5b. About 30 values of the line width w were taken between 0.1

mm and 3.0 mm for the curve fitting process.
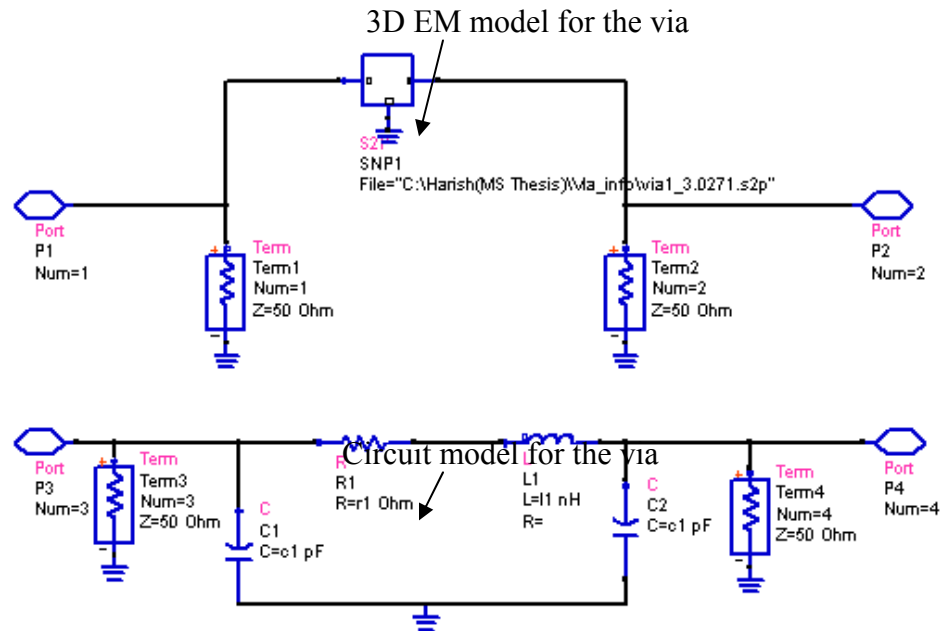
Fig 4.6 Optimization setup for the through-ground via model extraction

The via model was implemented on a back-to-back microstrip

platform with ε_r=2.2 and a substrate height h=31 mil for both dielectric layers

The thickness of the metallization is considered to be 0.7 mils. A time domain

solver was used for simulation [23]. The resistance, inductance and

capacitance variation versus the line width for the via model is shown in Fig

4.7. The dielectric losses have not been considered for this analysis. Metallic

losses have been taken into account and consequently the lumped equivalent

circuit of the via model as shown in Fig. 4.5b contains resistances, inductances and capacitances.
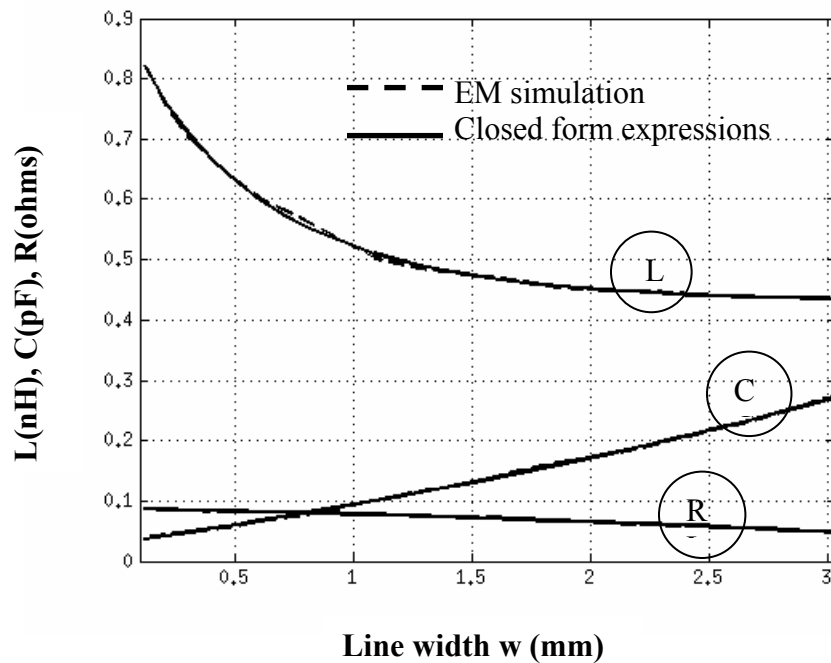
Fig 4.7 Inductance, capacitance and resistance vs. line width

As shown in Fig. 4.7, the R, L, C values obtained from the EM-based via models match very closely with those obtained from the closed form design equations (4.2-4.4).

4.4 Filter Design Procedure

The first step involves modeling of multiple coupled folded line bandstop and lowpass filters on a single layer microstrip platform. This procedure has already been explained in section 3.3. The next step involves

folding the single level folded line filter in one half along the width of it onto the bottom layer. Since the intermediate ground plane sufficiently isolates the top and the bottom metal layers, individual multiple-coupled sections on the same layer can be characterized to include only the coupling between various lines on the same layer. The top and bottom metal layers are interconnected by through-ground vias in terms of equivalent circuit models extracted from full-wave EM simulation. The folded line filter design carried out on a single layer provides an approximate range of line widths and separation between lines for various sections. The next step involves integration of the via models with the multiple coupled transmission line models as shown in Fig. 4.2 to get the reduced two-port network parameters of each multilayer folded line section.

For a given set of specifications for the bandstop/lowpass filters in terms of number of sections N, type of filter (maximally-flat or Chebyshev or equal-ripple), center frequency/ bandwidth/ cut-off frequency etc., the multi-layer folded line filter can be constructed by cascading the folded line filter sections, where each filter section includes a network model similar to that shown in Fig 4.2. Interconnecting lengths, corners and additional center stub lengths are included in the calculations while computing the reduced two-port network parameters of the folded line filter sections. The design flow for the multi-level folded line filters is summarized in Fig. 4.8. The overall footprint is greatly reduced in the case of the multi-level folded line lowpass/bandstop filters in comparison with the single level folded line filters which were shown

```
┌─────────────────────────────────────────┐
│              Specifications              │
└─────────────────────────────────────────┘
                    │
                    ▼
┌─────────────────────────────────────────┐
│  Lowpass filter prototype values gᵢ, i=0,1,2…. │
└─────────────────────────────────────────┘
                    │
                    ▼
┌─────────────────────────────────────────┐
│         Richard's transformations /      │
│            Kuroda's identities           │
└─────────────────────────────────────────┘
                    │
                    ▼
┌─────────────────────────────────────────┐
│      Impedance and frequency scaling     │
└─────────────────────────────────────────┘
                    │
                    ▼
┌─────────────────────────────────────────┐
│     Initial Length=λ/8 for lowpass       │
│     Initial Length=λ/4 for bandstop      │
└─────────────────────────────────────────┘
                    │
                    ▼
┌─────────────────────────────────────────┐
│     Conventional stub-loaded filter design │
└─────────────────────────────────────────┘
                    │
                    ▼
┌─────────────────────────────────────────┐
│   Single-level folded line filter dimensions │
└─────────────────────────────────────────┘
```

$$\text{Initial Length}=\lambda/8 \text{ for lowpass}$$
$$\text{Initial Length}=\lambda/4 \text{ for bandstop}$$

Specifications

Lowpass filter prototype values g_i, i=0,1,2….

Richard's transformations / Kuroda's identities

Impedance and frequency scaling

Initial Length=λ/8 for lowpass
Initial Length=λ/4 for bandstop

Conventional stub-loaded filter design

Single-level folded line filter dimensions

Through-ground via model extraction

Multi-level folded line filter sections without vias

Multi-level folded line filter sections with vias

Cascaded multi-level filter sections
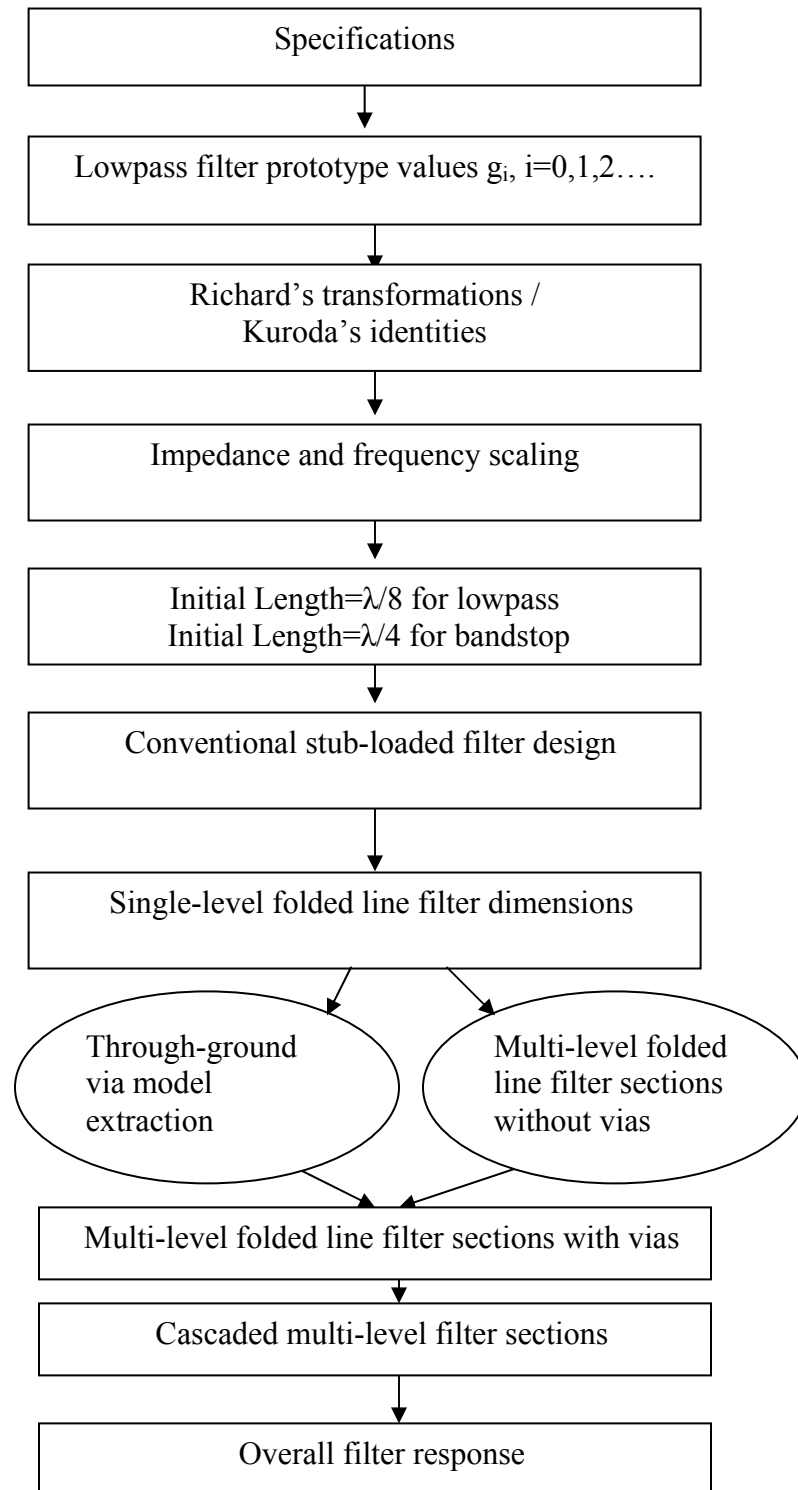
Overall filter response

Fig 4.8 Design flow for the multi-level folded line filters

in sections *3.4.1* and *3.4.2*. This is explained with the help of several examples in the following section.

4.5   Results and Discussion

4.5.1 BTB Microstrip bandstop filter

To demonstrate the design feasibility of this new design procedure explained in the earlier section, a 3-section multi-level folded line bandstop filter was designed for a maximally flat response at a center frequency of 1.5 GHz and a fractional bandwidth, $\Delta=0.3$. The folded line filter was implemented on a back-to-back microstrip platform with $\varepsilon_r=2.2$ and a substrate height h=31 mil for both dielectric layers. The thickness of the metallization is considered to be 0.7 mils.

The first phase of the design involves the modeling of a 3-section stub-loaded bandstop filter, the procedure for which was already explained earlier in chapter 2. All the transmission lines are of length $\lambda/4$ at the center frequency for this conventional stub-loaded bandstop filter. From the conventional stub-loaded filter, the design procedure for obtaining the single-level folded line filter was described in *3.4.1*. The individual sections of this single-level folded line filter are replaced with multi-level folded line filter sections as explained in section 4.4 of this chapter. The through-ground vias connect the top and bottom metal layers of the multi-level folded line filter sections. For each section of the multi-level folded line bandstop filter, the new

Multi-level folded line filter section 1

Conventional stub-loaded filter section 1

(a)

Multi-level folded line filter section 2

Conventional stub-loaded filter section 2
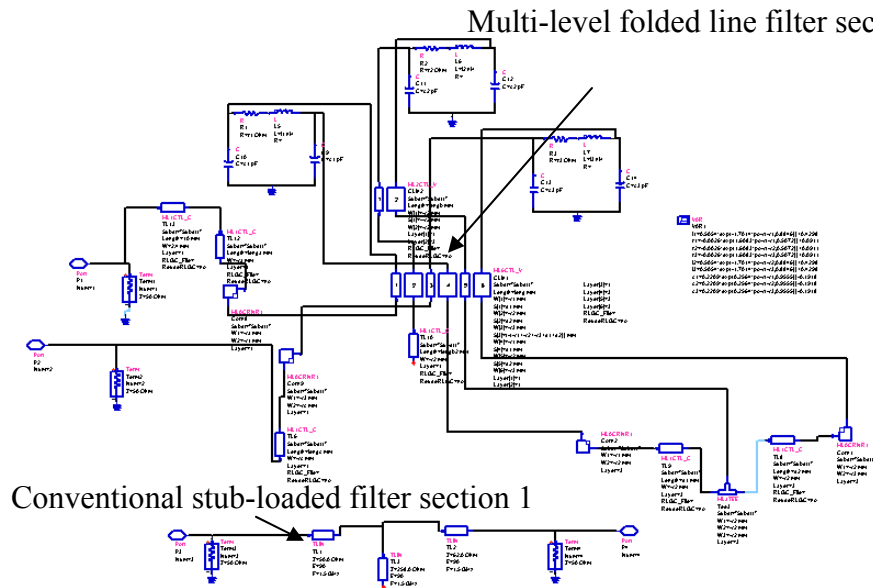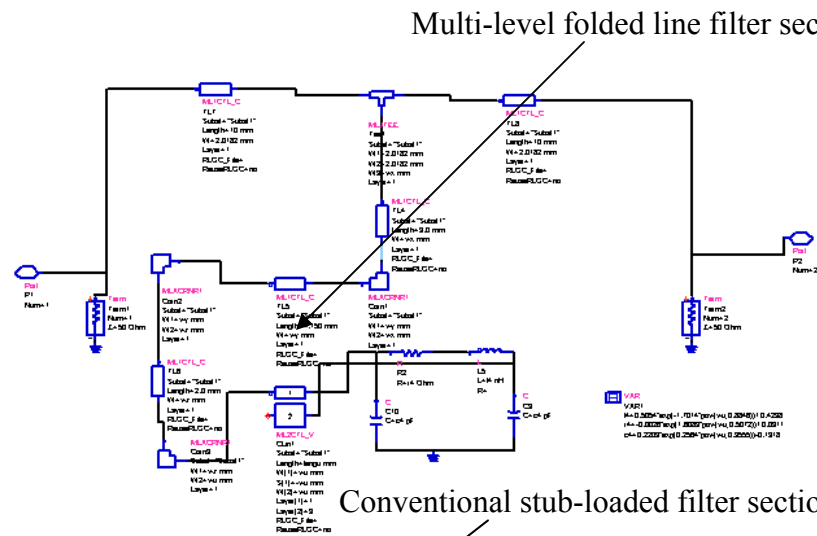
(b)

Fig 4.9 Optimization setup for the multi-level folded line filter sections with the through-ground via models included (a) Section 1 (b) Section 2

network model as shown in Fig 4.2 has been optimized separately to match the response of the corresponding section of the conventional stub-loaded filter. The optimization setup for the sections 1 and 2 of the multi-level folded line bandstop filter is shown in Fig. 4.9. Section 3 is the same as section 1 and has not been shown.

The design parameters for the individual optimization of each section are the widths w_1, w_2, w_3 of the three coupled lines, the spacings s_1, s_2 between the coupled lines, and the lengths of the coupled lines. Additionally, thin transmission lines were added to the open circuit shunt stubs of the first and third sections of the filter to be able to vary their lengths without changing the transmission line lengths as shown in Fig. 4.9a. The width w_0 and length l_0 of this line were also included as the design parameters for the optimization of the individual filter sections. The middle folded line filter section has been implemented as a serpentine line as shown in Fig. 4.9b to reduce the overall footprint. The Random/Quasi-Newton optimizer combination is employed for this purpose and required the use of Agilent EDA software [24]. The optimization band was 0.5-2.5 GHz with the center frequency of the bandstop filter being 1.5 GHz. The multi-level folded line filter was realized by combining all three individual filter sections.

Fig 4.10 shows the layouts for the designed 3-section multi-level folded line bandstop and the conventional stub-loaded filter design. The overhead view of the multi-level folded line bandstop filter is shown in Fig

4.10 and the 3-D view is shown in Fig 4.11. The line widths of the OC shunt

stubs of the first and third sections of the conventional bandstop filter are very

small (0.02 mm); hence the layout comparison as shown in Fig. 4.10 is not to

scale. The overall footprint observed in the case of the multi-level folded line

Smallest normalized width (w/h) =0.032

(a)

Top metal layer

Smallest normalized width
(w/h) =0.4

Bottom metal layer

(b)

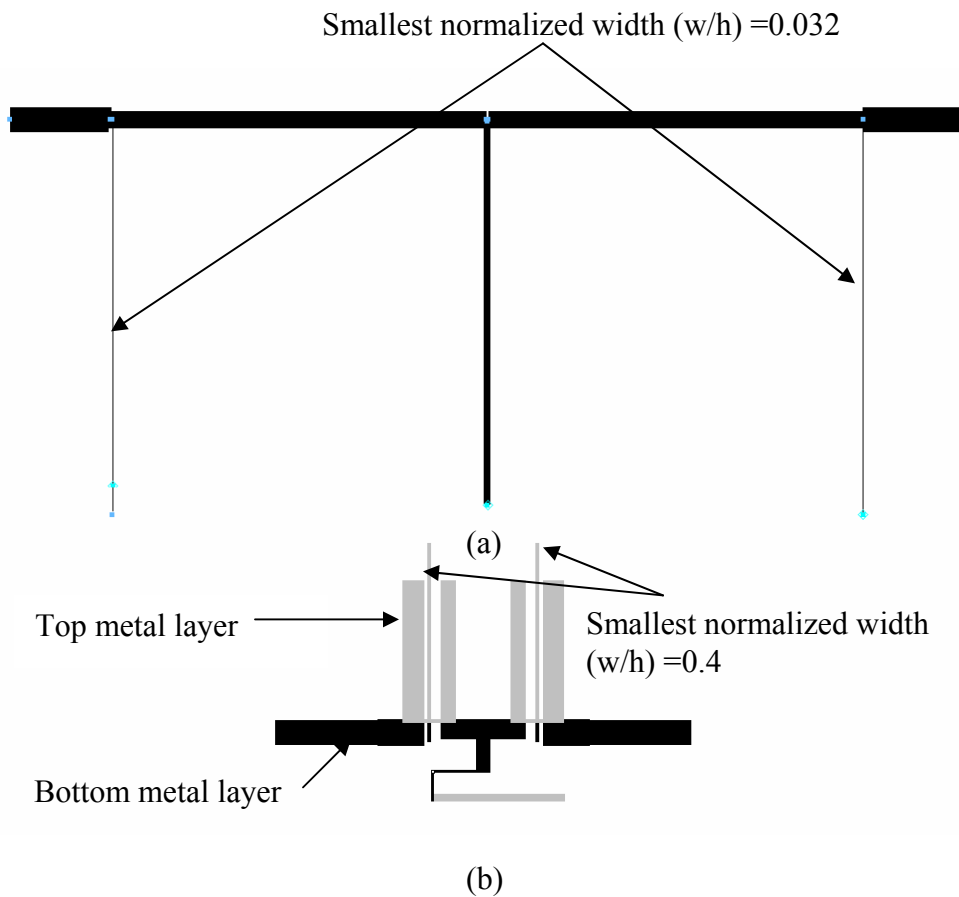**Fig 4.10 Physical layout comparison of the bandstop filters (Δ=0.3)
(a) Conventional stub-loaded filter (b) New multi-level folded line design**

bandstop filter is only 18% of the overall footprint of the conventional design

and 52 % of the overall footprint of the single-level folded line bandstop filter

which was shown in section *3.4.1*. Table 4.1 gives a comparison of the smallest

normalized width (w/h) of the conventional design and the multi-level folded-line design. It can be seen that the normalized conductor widths for the new multi-level folded design are much larger (0.4 versus 0.032). This allows practical realization of the multi-level folded line filters with less stringent dimensional tolerances.

Δ=0.3	Conventional Bandstop	Single Level Folded Line Bandstop	Multi Level Folded Line Bandstop
Smallest normalized width (w/h)	0.032	0.5	0.4
Overall footprint	2948.2 sq mm	1015.1 sq mm	531.8 sq mm
Footprint comparison	100 %	34 %	18 %

Table 4.1 Footprint and critical conductor width comparison for the folded line bandstop filters (Δ =0.3)

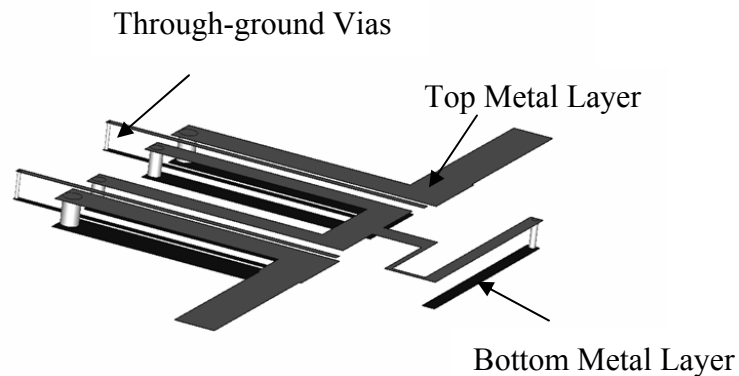**Fig 4.11 3-D view of the new multi-level folded line design (Δ=0.3) with the ground plane hidden for better visibility**

Fig. 4.12 shows a comparison of the theoretical results with the full-wave 3D EM simulation [23]. There is a good agreement in the insertion loss response,

the return loss values were observed to be below -20 dB in the lower and upper passbands. The slight deterioration in the results can be attributed to the mutual coupling between the multi-level folded line filter sections which was only taken into account in the full wave EM simulation.
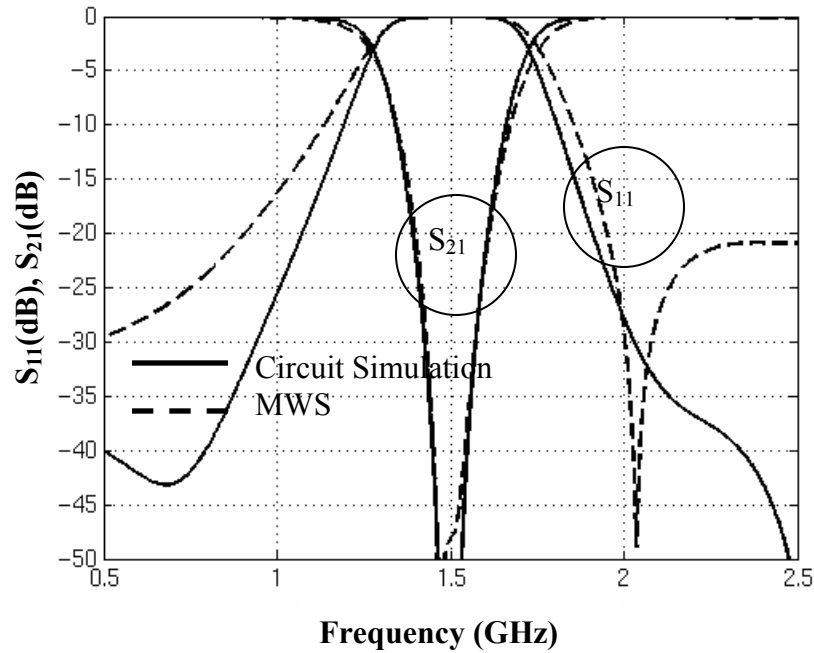
Fig 4.12 Multi-level folded line bandstop filter response (f_0=1.5 GHz, Δ=0.3)

4.5.2 BTB Microstrip lowpass filter

Next, a 3-section lowpass filter was designed for a maximally flat response with a cut-off frequency of 1.5 GHz, and with the substrate specifications remaining the same as mentioned above. The conventional stub-loaded filter can be derived starting with the lowpass prototype values g_i i=0,1,2.., following the procedure described in chapter 2. The length of the transmission lines in the case of the conventional stub-loaded lowpass filter

being $\lambda/8$ at the cut-off frequency. From the conventional stub-loaded filter, the design procedure for the multi-level folded line lowpass filter is similar to that of the multi-level folded-line bandstop filter. Thus, the physical dimensions of the folded line filter sections are obtained and then these are cascaded to give the overall filter response.

The characteristic impedance values of the lowpass filter sections of the conventional stub-loaded filter are provided in Table 3.6. The central stub has a characteristic impedance of 25 ohms. When the filter is implemented on a microstrip platform with ε_r=2.2 and substrate height h=31 mil, this stub is extremely wide (w/b ~8). This has been replaced by two parallel coupled stubs on each layer and interconnected by through-ground vias in the case of the multi-level folded line lowpass filter, implemented in a back-to-back microstrip platform. The widths and central spacing of the parallel-coupled stubs were optimized to provide a close agreement in response with that of the conventional single stub design shown as section 2 in Fig 4.13b. The optimization setup for the sections 1 and 2 of the multi-level folded line lowpass filter is shown in Fig. 4.13. Section 3 is the same as section 1 and has not been shown. The Random/Quasi-Newton optimizers were used in that order for the optimizations. For this purpose, Agilent EDA [24] software was used.

Multi-level folded line filter section 1

Conventional stub-loaded filter section 1

(a)

Multi-level folded line filter section 2
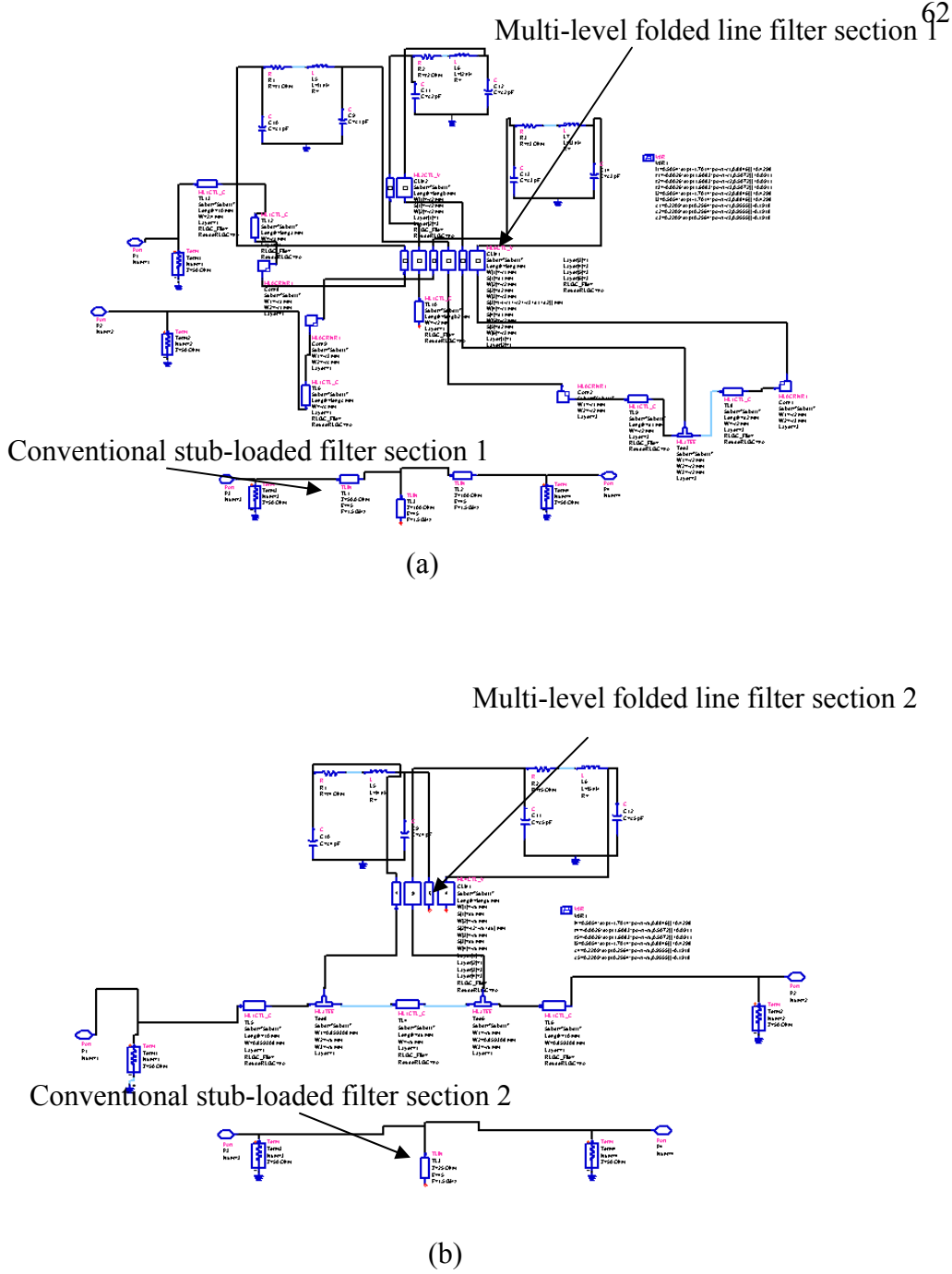
Conventional stub-loaded filter section 2

(b)

Fig 4.13 Optimization setup for the multi-level folded line filter sections with the through-ground via models included (a) Section 1 (b) Section 2

The footprint comparison of the multi-level folded line configuration and the conventional lowpass filter is shown in Fig 4.14. The overhead view of the multi-level lowpass filter is shown in Fig 4.14 and the 3-D view is shown in Fig 4.15. The physical layout comparison as shown in Fig 4.14 is to scale. The overall footprint of the multi-level folded line lowpass filter is only 31% of the overall footprint of the conventional stub-loaded lowpass filter and 44% of the overall footprint of the single-level folded line lowpass filter which was shown in section *3.4.2*.

Table 4.2 gives a comparison of the largest normalized width (w/h) of the conventional design and the multi-level folded-line design. From Table 4.2, it can be seen that the normalized conductor widths for the new multi-level folded line design are much smaller (3.21 versus 7.9).

Fig 4.16 shows the circuit simulation results in comparison with the full wave 3D EM simulation results [23] for the multi-level folded line lowpass filter. The return loss response shows a good agreement between the circuit and full wave EM simulations. The insertion loss is in good agreement up to the cutoff frequency (f_c =1.5 GHz). The slight deterioration in the insertion loss response above the cut-off frequency can be attributed to the mutual coupling between the multi-level folded line filter sections which were only taken into account in the full wave EM simulation and are more predominant at frequencies higher than the cut-off frequency of 1.5 GHz.

Largest normalized width (w/h) =7.9

(a)

Largest normalized width (w/h) =3.2
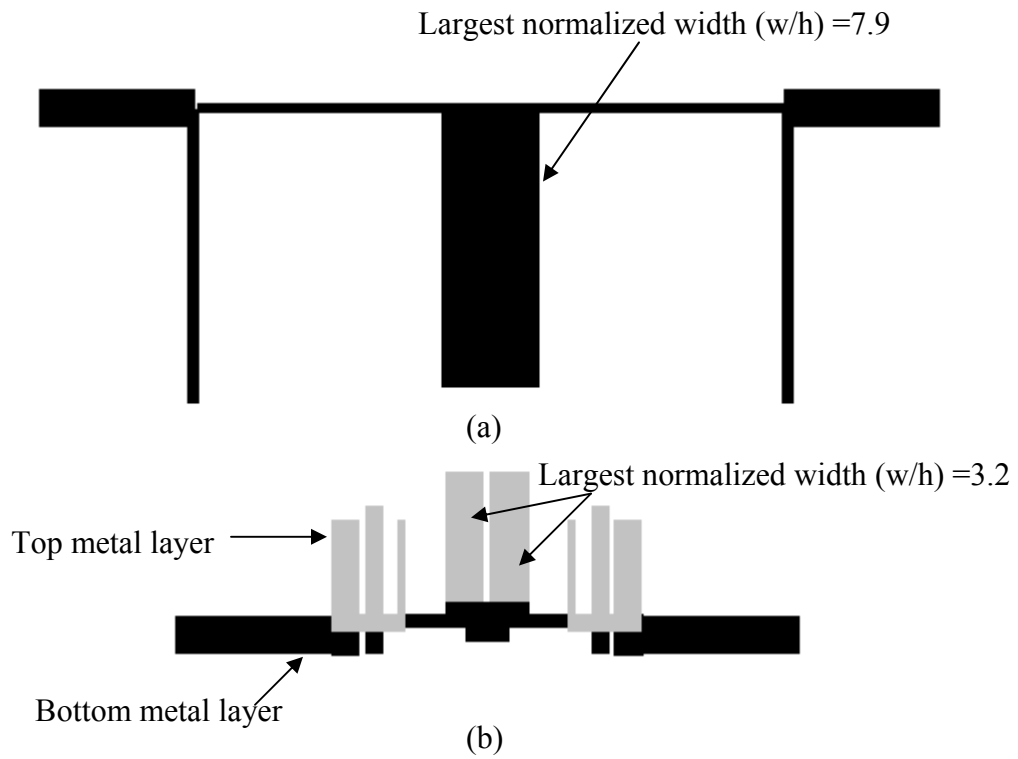
Top metal layer

Bottom metal layer

(b)

Fig 4.14 Physical layout comparison of the lowpass filters (f_c=1.5 GHz)
(a) Conventional stub-loaded filter (b) New multi-level folded line design

Through-ground Vias

Top Metal Layer

Bottom Metal Layer
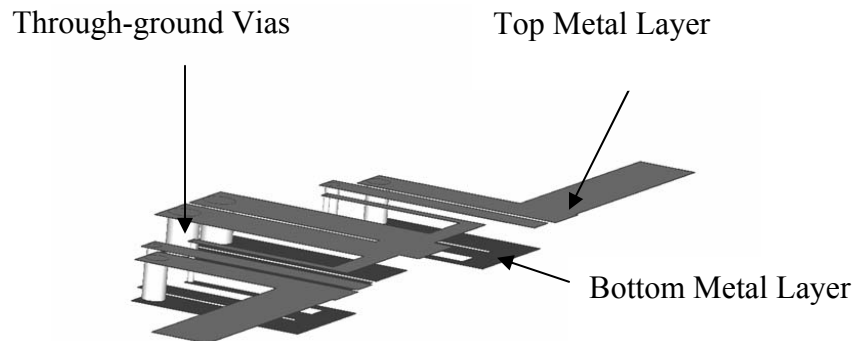
Fig 4.15 3-D view of the new multi-level folded line design (f_c=1.5 GHz)
with the ground plane hidden for better visibility

f_c=1.5 GHz	Conventional Lowpass	Single Level Folded Line Lowpass	Multi Level Folded Line Lowpass
Largest normalized width (w/h)	7.9	3.6	3.2
Overall footprint	754.9 sq mm	634.6 sq mm	234.8 sq mm
Footprint comparison	100 %	71 %	31 %

Table 4.2 Footprint and critical conductor width comparison for the folded line lowpass filters (f_c =1.5 GHz)

Fig 4.13 Multi-level folded line lowpass filter response (f_c=1.5 GHz)

5. EXPERIMENTAL VALIDATION

5.1   Introduction

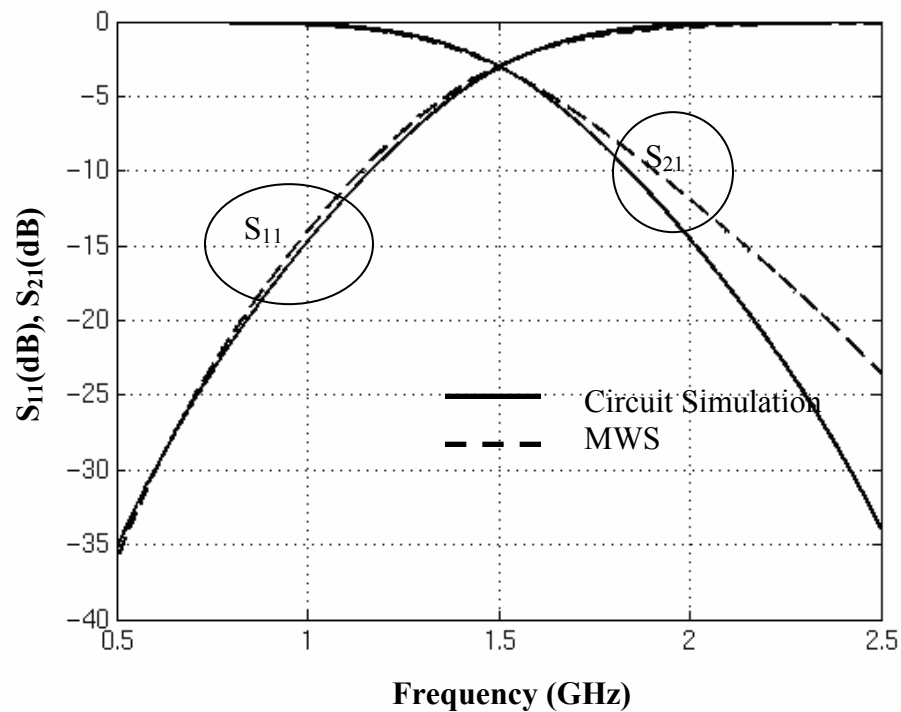In this chapter, the proposed folded line bandstop and lowpass filter configurations have been validated with the measurement results. We shall demonstrate that the measured responses of the folded line filters in single and multi-layer environment match closely with the corresponding theoretical responses as well as with the full wave EM simulation results. All the fabrications have been carried out in-house and the slight discrepancies in the measurement results can be attributed to the fabrication tolerances of the PCB based milling and drilling processes.

5.2   Experimental Results for Single-Level Filters

The 3-section single-level folded line bandstop filter (f_0=1.5GHz, Δ=0.3) described in section *3.4.1* was fabricated on Roger's RT Duroid 5880 substrate of 31 mil thickness. The structure was fabricated using an in-house milling machine facility and was tested on an HP 8722C vector network analyzer. A photograph of the fabricated folded line bandstop filter is shown in Fig 5.1.

Fig 5.2 shows the measurement results in comparison to the theoretical results, as well as with full wave EM simulation using CST Microwave Studio® [23] and Agilent Momentum [24]. The measured results

are in good agreement with the theory as well as with full-wave EM simulation

[15] [16]. The slight discrepancies in the measurement results can be attributed

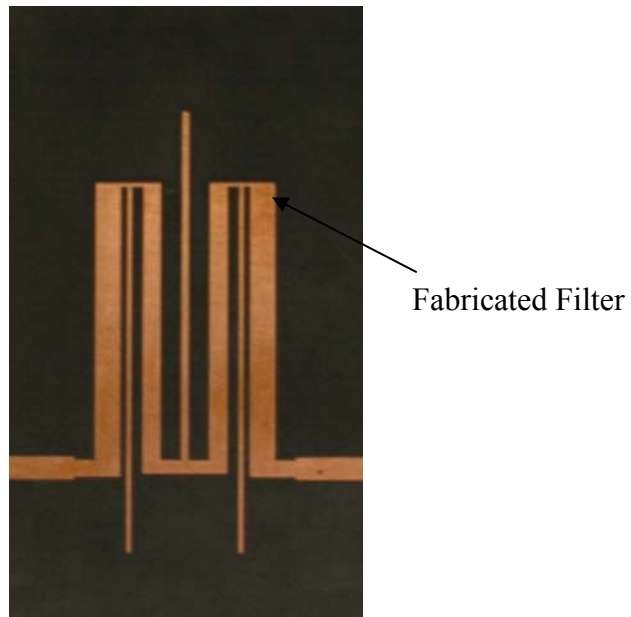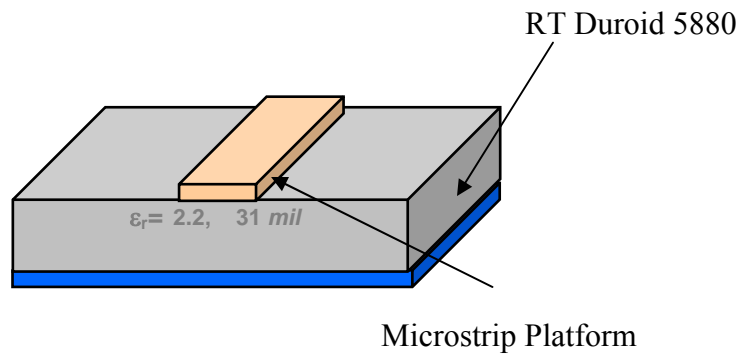to the fabrication tolerances of the PCB based milling and drilling processes.

Fig 5.1 Cross-section and photograph of the fabricated single level folded line bandstop filter (f_0 =1.5 GHz, Δ=0.3)
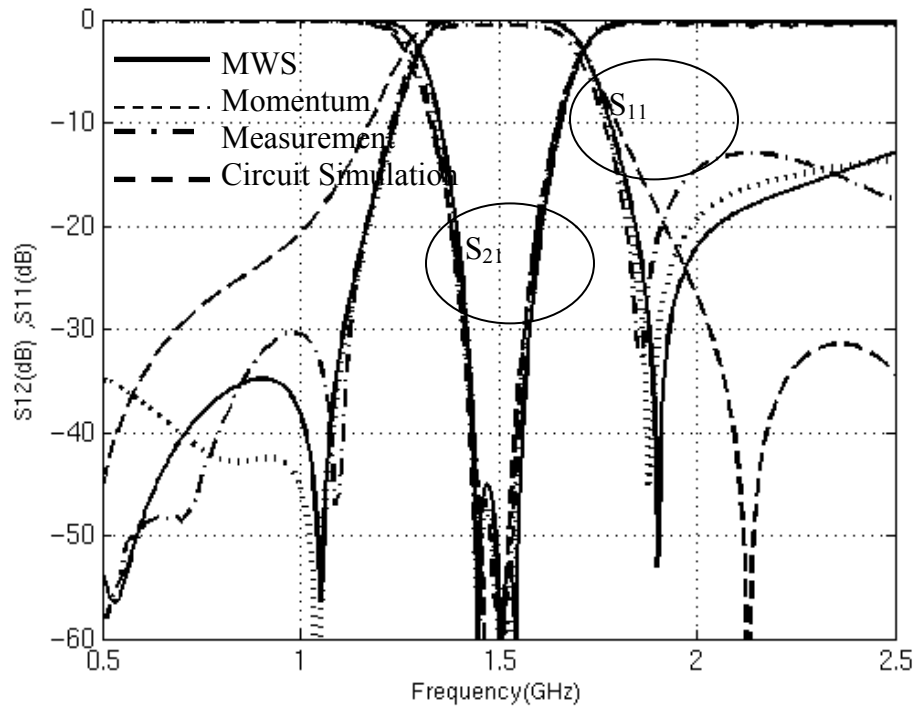
Fig 5.2 Measurement results for the fabricated single-level folded line bandstop filter shown in Fig. 5.1

The 3-section single-level folded line lowpass filter (f_c=1.5GHz) described in section *3.4.2* was also fabricated on Roger's RT Duroid 5880 substrate of 31 mil thickness. The structure was fabricated using the in-house milling machine facility and was tested on a HP 8722C vector network analyzer. A photograph of the fabricated folded line lowpass filter is shown in Fig 5.3. All the fabrications which include the drilling and milling processes and the measurements were done in-house. The vector network analyzer was calibrated in order to give the correct network parameters i.e the scattering parameters. The most popular methods of calibration are the Thru-Reflect-Line (TRL) and the Short-Open-Load-Reciprocal (SOLT) respectively.

RT Duroid 5880

ε_r= 2.2,   31 *mil*

Microstrip Platform
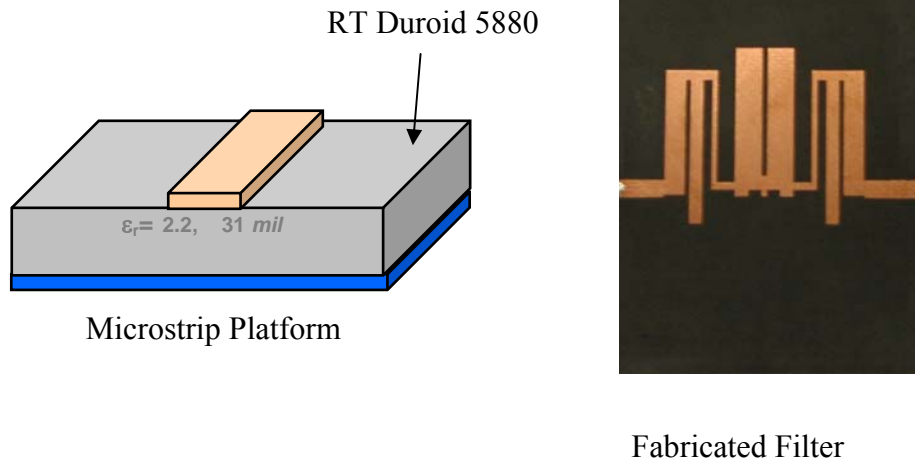
Fabricated Filter

Fig 5.3 Cross-section and photograph of the fabricated single-level folded line lowpass filter (f_c =1.5 GHz)

Fig 5.4 shows the measurement results in comparison to the theoretical results, as well as with full wave EM simulation using CST Microwave Studio® [23] and Agilent Momentum [24]. The measured results are in good agreement with the theory as well as with full-wave EM simulation.

5.3 Experimental Results for Multi-Level Filters

The 3-section multi-level folded line bandstop filter (f_0=1.5GHz, Δ=0.3) described in section *4.5.1* was fabricated on two back-to-back layers of Roger's RT Duroid 5880 substrate of 31 mil thickness. The structure was fabricated using the in-house milling machine facility. The transmission line widths for this design were 2.1 mm, 0.4 mm, 1.5 mm and 0.7 mm respectively.
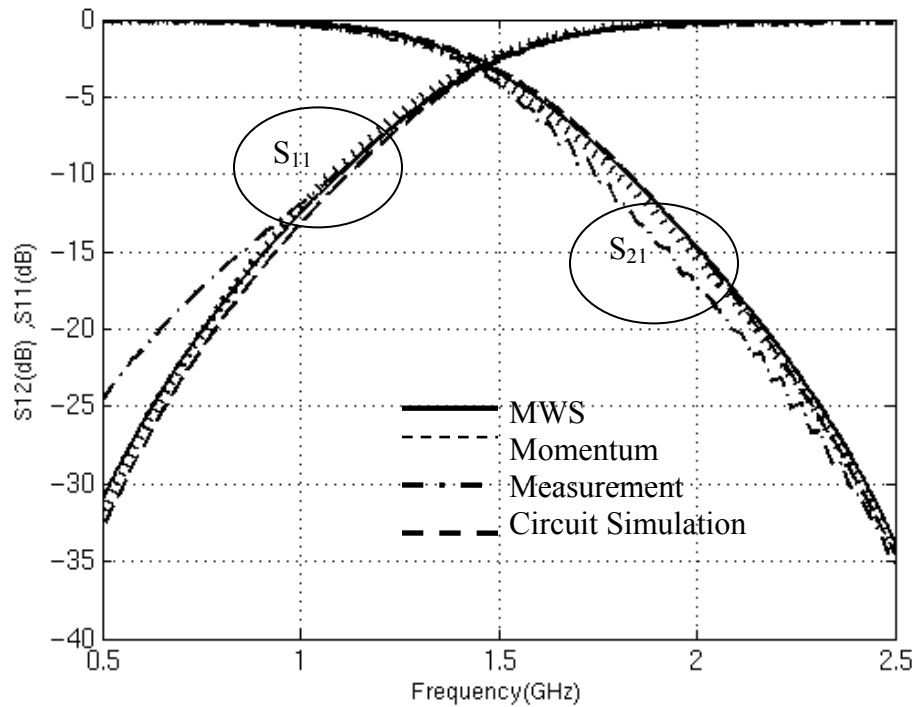
Fig 5.4 Measurement results for the fabricated single-level folded line lowpass filter shown in Fig. 5.3

The via diameters were chosen to be approximately one half of the above line widths. The ground plane holes were chosen to be 0.4 mm larger in diameter than the via holes for all widths. Using the in-house drilling facility, the ground plane holes were first created. The diameters of the drilling bits used were approximately equal to the diameters of the corresponding holes in the ground plane. To interconnect the top and bottom metallization layers, copper wires with diameters equal to the via diameters were chosen. For this purpose, 18, 30, 22 and 28 gauge wires with the insulation removed were used. Copper guage wires with even numbered wire gauges are readily available and were thus preferred over odd numbered wire gauges.

ε_r= 2.2,   31 *mil*

ε_r= 2.2,   31 *mil*

RT Duroid 5880
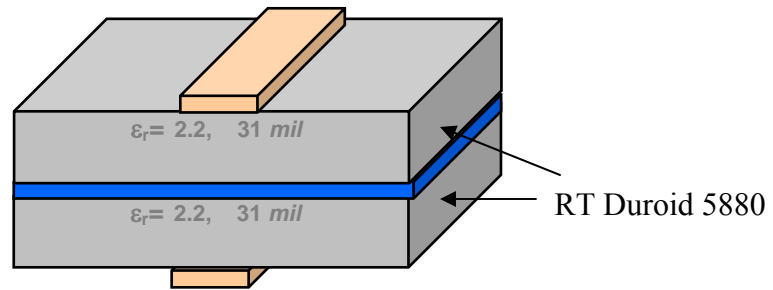
BTB microstrip platform
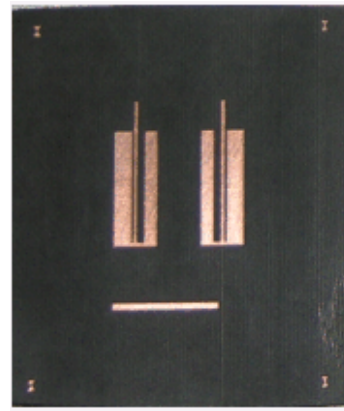
Top metal layer

Bottom metal layer

Fig 5.5 Cross-section and photograph of the fabricated multi-level folded line bandstop filter (f_0 =1.5 GHz, Δ=0.3)

The fabricated multi-level folded line bandstop filter was tested on an HP 8722C vector network analyzer. A photograph of the fabricated folded line bandstop filter is shown in Fig 5.5. Both the top and bottom metallization layers are shown in the figure.

Fig 5.6 shows the measurement results in comparison to the theoretical results, as well as with full wave 3D EM simulation using CST Microwave Studio® [23]. The measured results are in good agreement with the theory as well as with full-wave EM simulation. The slight discrepancy in the insertion loss and return loss responses can be attributed to the fabrication tolerance of the PCB based milling and drilling processes respectively.

Fig 5.6 Measurement results for the fabricated multi-level folded line bandstop filter shown in Fig. 5.5

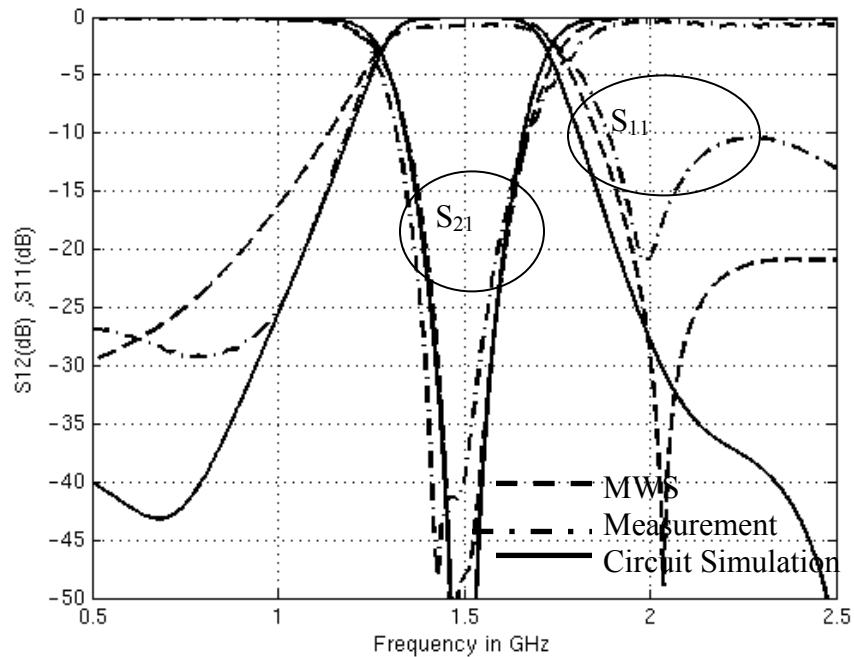The 3-section multi-level folded line lowpass filter (f_c=1.5GHz) described in section *4.5.2* was also fabricated on two back-to-back layers of Roger's RT Duroid 5880 substrate of 31 mil thickness. The transmission line widths for this design were 1.8 mm, 1.1 mm, 0.4 mm and 2.5 mm respectively.

The structure was fabricated using a similar procedure described for the multi-level bandstop filter with the help of the in-house milling machine facility and was tested on an HP 8722C vector network analyzer. A photograph of the fabricated folded line lowpass filter is shown in Fig 5.7.

Fig. 5.8 shows the measurement results in comparison to the theoretical results, as well as with full wave 3D EM simulation using CST Microwave Studio® [23]. The measured results are in good agreement with the theory as well as with full-wave EM simulation.

$\varepsilon_r = 2.2, \quad 31\ mil$

$\varepsilon_r = 2.2, \quad 31\ mil$

RT Duroid 5880

BTB microstrip platform

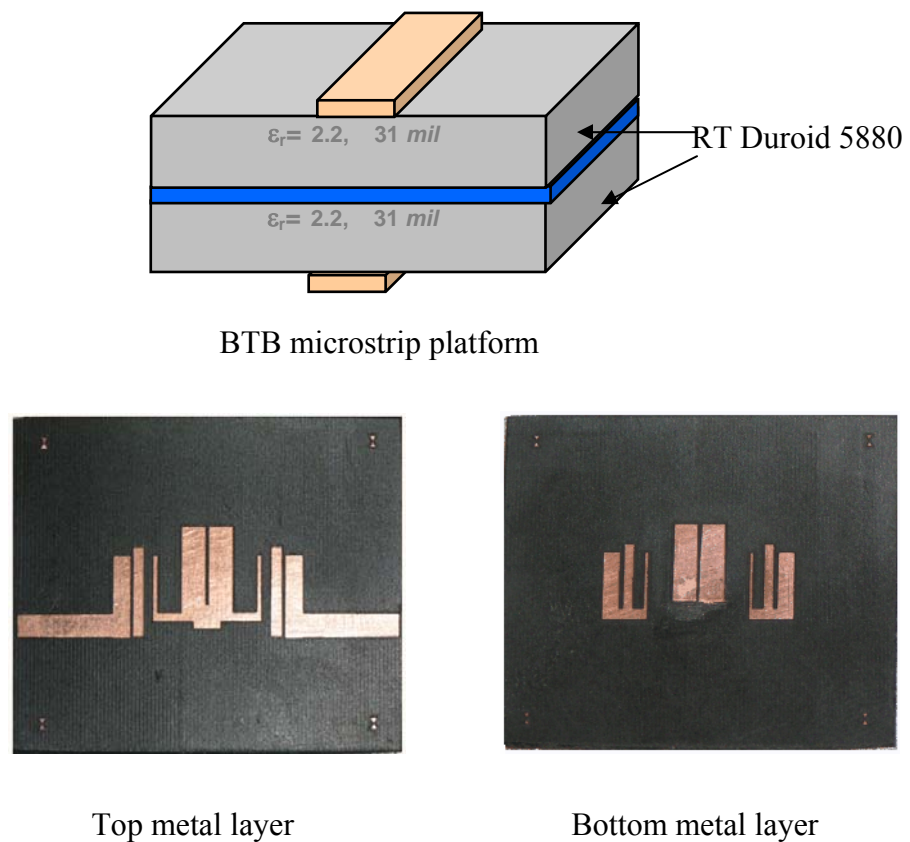Top metal layer   Bottom metal layer

Fig 5.7 Cross-section and photograph of the fabricated multi-level folded line lowpass filter (f_c =1.5 GHz)
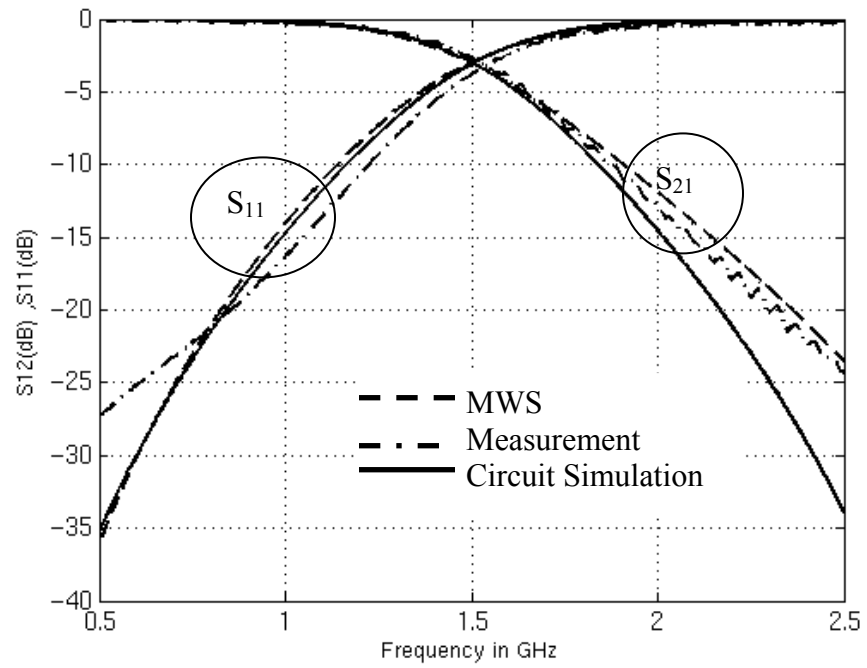
Fig 5.8 Measurement results for the fabricated multi-level folded line lowpass filter shown in Fig. 5.7

6. CONCLUSIONS

6.1 Conclusions

Compact single-level folded line bandstop and lowpass filters have been reported. A common design procedure was employed for designing both bandstop and lowpass folded line filters. The transmission line and stub sections of the conventional design were replaced by the folded line filter sections to achieve compact footprint. For a given set of filter specifications, physical parameters of each folded line E-section were obtained by comparing the reduced two-port network parameters with those obtained from the lowpass filter prototype design. Bandstop and lowpass filters were designed at 1.5 GHz with a maximally flat response and have been fabricated on a microstrip platform with ε_r=2.2 and substrate height h=31 mil. The overall footprint of the folded line bandstop filter is only 34% of the overall footprint of its conventional counterpart; the overall footprint of the folded line lowpass filter is 71% of its conventional counterpart. The normalized conductor widths for the new folded line bandstop design are much larger (0.5 versus 0.032) and the conductor widths for the new folded line lowpass design are much smaller (3.63 versus 7.9). Thus, the folded line designs have practical dimensions for a physical realization, thereby eliminating the problem of having very narrow or very wide line widths as in the case of the conventional filter configurations. The measurement results are in good agreement with the theoretical results, as

well as full wave EM simulation using CST Microwave Studio® [23] and Agilent Momentum [24].

Compact multi-level folded line bandstop and lowpass filters have also been developed. A simple design methodology for designing these filters has been presented. The transmission line and stub sections of the conventional design were replaced by multi-level folded line filter sections to achieve greater reduction in the footprint in comparison with the single-level folded line filters. An equivalent network model consisting of the interconnection of multiple coupled lines on each layer using through -ground vias has been used to realize the multi-level filter configurations. A back-to-back microstrip was considered for this purpose. The ground plane sandwiched between the dielectric layers serves to sufficiently isolate the top and bottom metal layers and thus aids in the design of these filters. Any slight misalignment of the top and bottom metallization layers would not adversely affect the filter response because of the presence of the ground plane. The through-ground vias used to interconnect the top and bottom metallization layers have been obtained from full wave EM simulation. The corresponding equivalent circuit model parameters for the through-ground via models have been determined by a direct comparison of the scattering parameters of the via model results obtained from EM simulation with the network parameters of the via model.

Bandstop and lowpass filters were designed at 1.5 GHz with a maximally flat response and have been fabricated on a back-to-back microstrip

platform with ε_r=2.2 and substrate height h=31 mil for both dielectric layers. The overall footprint of the multi-level folded line bandstop filter is only 18% of the overall footprint of its conventional counterpart and 52% of the overall footprint of the single-level folded line bandstop filter. The normalized conductor widths for the new multi-level folded line bandstop design are much larger (0.4 versus 0.032) when compared to the conventional design. The overall footprint of the multi-level folded line lowpass filter is only 34% of the overall footprint of its conventional counterpart and 44% of the overall footprint of the single-level folded line lowpass filter. The conductor widths for the new multi-level folded line lowpass design are much smaller (3.21 versus 7.9) when compared to the conventional design. Thus, the multi-level folded line designs have practical dimensions for a physical realization, thereby eliminating the problem of having very narrow or very wide line widths as in the case of the conventional filter configurations. The measurement results are in good agreement with the theoretical results, as well as full wave 3D EM simulation using CST Microwave Studio® [23]. The new filter designs presented are useful for RF wireless applications in the 1-10 GHz range.

6.2   Further Research

Potential avenues for further research in this area of filter synthesis and design are as follows. Closed form design equations can be developed for the line widths, spacing and length of the coupled lines of the folded line filter

sections in terms of the lowpass prototype values. This would eliminate the need for performing optimizations to match the response of the conventional stub loaded designs.

Alternatively, Artificial Neural Network models (ANN) can be developed. Artificial neural networks are emerging as a fast and powerful alternative to time-consuming EM computation [28] - [30]. They are used for RF and microwave characterization, modeling and design. From the microwave data available, the neural network model is trained and used to further enhance the microwave design. Artificial neural networks are best used in scenarios where EM computations are expensive, in modeling new components where closed form expressions are unavailable. This method is particularly useful in optimizations and parameter sweeps which are otherwise very time consuming. The results from the artificial neural network models can be used in the synthesis of the bandstop and lowpass microwave filters.

Finally, the design methodology used in the case of the multi-level folded line bandstop and lowpass filters using the through-ground vias can be extended to other passive microwave structures like toroidal inductors, directional couplers, power dividers etc.

BIBLIOGRAPHY

[1]   A. Sutono, D. Heo, Y.J Chen and J. Laskar, "High-Q LTCC-based development," *IEEE Trans. Microwave Theory Tech.,* vol. 49, pp. 1715-1724, Oct 2001.

[2]   C.Q. Scrantum and J.C Lawson, "LTCC Technology: Where we are and where we're Going," June 2000.

[3]   P. Pieters, K. Vaesen, S. Brebels, S. Mahmoud, W. Raedt, E. Byne and R.P Mertens, "Accurate Modeling of High-Q Spiral Inductors in Thin-Film Multilayer Technology for Wireless Telecommunication Applications," *IEEE Trans. Microwave Theory Tech.*, vol. 9, pp. 589 599, Apr 2001.

[4]   P. Pieters, S. Brebels and E. Beyne, "Integration of Passive Components for Microwave Filters in MCM-D," *Proc. Int. Multichip Modules Conf., Denver, CO,* pp. 357-362, 1997.

[5]   D.M. Pozar, *Microwave Engineering,* 2nd ed. New York: Wiley, 1998.

[6]   G.L Matthaei, L. Young and E.M.T Jones, *Microwave Filters, Impedance Matching Networks and Coupling Structures.* New York: McGraw-Hill, 1964.

[7]   J.A.G Malherbe, *Microwave Transmission Line Filters,* Artech House, Dedham, Mass., 1979.

[8]   J. Helszajn, *Microwave Planar Passive Circuits and Filters,* John Wiley & Sons.

[9]   R.K Settaluri, A. Weisshaar and V.K. Tripathi, "Compact Multi-level Folded-line Bandpass Filters," *IEEE Trans. Microwave Theory Tech.*, Oct 2001.

[10] R.K Settaluri, A. Weisshaar, C. Lim and V.K. Tripathi, "Design of Compact Multi-level Folded-line RF Couplers," *IEEE Trans. Microwave Theory Tech.,* vol. 47, No. 12, Dec 1999.

[11] C. Cho and K.C. Gupta, "Design Methodology for Multi-layer Coupled Line Filters," *IEEE MTT-S International Microwave Symposium,* June 1997.

[12] W. Menzel and W. Schwab,“ Compact Multilayer Filter Structures for Coplanar MMIC's,” *IEEE Microwave and Guided Wave Letters ,* vol. 2 , No. 12, Dec 1992.

[13] R.E. Collin, *Foundations for Microwave Engineering,* Second Edition, McGraw-Hill, N.Y., 1992.

[14] W.A. Davis, *Microwave Semiconductor Design,* Van Nostrand Reinhold, N.Y., 1984.

[15] H. Peddibhotla and R.K. Settaluri, “Compact Folded-line Bandstop and Lowpass Filters,” *Micro. Optical Tech. Letters,* vol. 42, issue 1, pp. 44-46, May 2004.

[16] H. Peddibhotla and R.K. Settaluri, “Miniaturized High Performance Lowpass and Bandstop Filters for Wireless Applications,” *Proc. IMAPS Conf. on Ceramic Interconnect Tech.,* Apr. 2003.

[17] C. Lim, R.K. Settaluri, A. Weisshaar and V.K. Tripathi, “Compact Folded-Line RF Power Dividers,” *Proceedings, International Symposium on Microelectronics, IMAPS.,* Jan 2001.

[18] K. Gururajan, H. Peddibhotla and R.K. Settaluri, “New Configurations for High Frequency Capacitors and Composite Structures for Embedded Passive and RFIC Applications.” *Proc. International Symposium on Microelectronics, IMAPS.,* Sep. 2002.

[19] K. Gururajan, H. Peddibhotla and R.K. Settaluri, “New Configurations of Single and Multi-Level Bandpass Filters with Excellent Harmonic Suppression,” *Micro. Optical Tech. Letters,* vol. 39, issue 6, pp. 490-493, Dec 2003.

[20] A. Tripathi and V.K Tripathi, “A configuration oriented SPICE model for multiconductor transmission lines in an inhomogeneous medium,” *IEEE Trans. Microwave Theory Tech.,* vol. 46, pp, 1997- 2005, Dec 1998.

[21] V.K. Tripathi, “On the Analysis of Symmetric Three-line Microstrip Circuits,” *IEEE Trans Microwave Theory Tech.,* vol. 25, pp. 726-729, Sept 1977.

[22] K.D Marx and R.I. Eastin, “A Configuration Oriented SPICE model for multiconductor transmission lines with homogeneous dielectrics,” *IEEE Trans Microwave Theory Tech.,* vol. 38, pp. 1123-1129, Aug1990.

[23] CST Microwave Studio® version 5.1.3, Computer Simulation Technology, Boston, Massachusetts, USA.

[24] Advanced Design System version 2004A, Agilent Technologies, Santa Rosa, California, USA.

[25] C. Lim, R.K. Settaluri, V.K. Tripathi and A. Weisshaar, "Compact Singlelevel and Multilevel Folded-line RF Power Dividers," *Microwave Optical. Tech. Letters,* vol. 39, issue 3, pp. 187-189, Nov 2003.

[26] Z. Chen, "Fast Computation of Multiport Parameters of Multiconductor Coupled Microstrip Lines," *IEEE Trans. Microwave Theory Tech.,* vol. 43, pp. 1393-1395, Jun 1995.

[27] I. Bahl, Lumped Elements for RF and Microwave Circuits, vol. 88, pp. 284-286, Artech House 2003.

[28] Q.J. Zhang and K.C. Gupta, Neural Networks for RF and Microwave Design, Artech House 2000.

[29] P.M. Watson and K.C Gupta, "EM-ANN Models for Microstrip Vias and Interconnects in Multilayer Circuits," *IEEE Trans. Microwave Theory. Tech.,* vol. 44, pp. 2495-2503, Dec 1996.

[30] G.L. Creech et al., "Artificial Neural Networks for Fast and Accurate EM-CAD of Microwave Circuits," *IEEE Trans. Microwave Theory and Techniques,* vol. 45, pp. 794-802, May 1997.

[31] R.K Settaluri, G. Sundberg, A. Weisshaar and V.K. Tripathi, "Compact Folded-Line Rat Race Hybrid Couplers," *IEEE Transactions on Microwave and Guided Wave Letters,* vol. 10, No. 2 ,pp. 61-63, Feb 2000.

[32] R.K. Settaluri, "Miniaturized Single/ Multi-Level Bandpass Filters for LTCC Applications," *Proc. 204 th ACERs Conference of Electrochemical Society,* Oct 2003.

[33] V.K. Tripathi, R.K. Settaluri, and A. Weisshaar, "Multilevel Embedded Passives for RF Modules," *2nd Int. Academic Conference at PRC, Georgia Tech Atlanta,* Mar 1999.